Spatiotemporal Variability of the South Pacific Convergence Zone Fresh Pool Eastern Front from Coral-Derived Surface Salinity Data

EMILIE P. DASSIÉ

Laboratoire d'Océanographie et du Climat: Expérimentations et Approches Numériques, LOCEAN-IPSL, UMR 7159 Sorbonne Université/IRD/CNRS/MNHN, Université Pierre et Marie Curie, Paris, France, and Lamont-Doherty Earth Observatory, Columbia University, Palisades, New York

AUDREY HASSON, MYRIAM KHODRI, AND NICOLAS LEBAS

Laboratoire d'Océanographie et du Climat: Expérimentations et Approches Numériques, LOCEAN–IPSL, UMR 7159 CNRS/UPMC/IRD, Université Pierre et Marie Curie, Paris, France

BRADDOCK K. LINSLEY

Lamont-Doherty Earth Observatory, Columbia University, Palisades, New York

(Manuscript received 8 February 2017, in final form 15 November 2017)

ABSTRACT

Direct observations indicate a southeastward expansion of the South Pacific convergence zone (SPCZ) fresh pool and a freshening trend since the 1970s. Understanding decadal and longer-term variability of the SPCZ fresh pool and of the salinity front located at its southeastern margin has been limited by the scarcity of instrumental sea surface salinity (SSS) measurements. This study uses coral $\delta^{18}O$ as a proxy for SSS to extend the salinity record back to the 1880s, from three different locations across the SSS front: Fiji, Tonga, and Rarotonga (FTR region). High percentages of observed SSS variance are explained by multicoral $\delta^{18}O$ mean composite at each site. At the interannual time scale, the salinity front displacement over the last 200 years follows the El Niño–Southern Oscillation (ENSO) index. The different El Niño flavors are observable in the amplitude of the salinity front interannual displacement. However, no significant changes in either the frequency or the amplitude of its displacements were observed. At longer time scales, the timing and magnitude of the freshening trend vary among sites. The earliest freshening onset of about -0.06 psu decade^{-1} is detected in Fiji (around 1865), then Rarotonga (around 1939), and Tonga (around 1982). The role of atmospheric freshwater fluxes on SSS variability is evaluated by comparing coral SSS to historical precipitation data. The results suggest that, despite the known influence of the interdecadal Pacific oscillation (IPO) negative phases on increasing atmospheric freshwater fluxes and lowering SSS in the FTR region, ocean dynamics has a dominant influence at decadal time scale and in the onset of freshening trends.

1. Introduction

The South Pacific convergence zone (SPCZ) is one of the major atmospheric features of the Southern Hemisphere. It is a persistent band of atmospheric convergence associated with deep convection and high rainfall. It extends southeast from the western Pacific warm pool (WPWP), where it is merged with the intertropical convergence zone (ITCZ), deep into the subtropical South Pacific (e.g., Vincent 1994; Vincent et al. 2011).

The SPCZ position is associated with a large area of relatively low sea surface salinity (SSS) waters, hereafter called the SPCZ fresh pool (Gouriou and Delcroix 2002; Yu 2011; Skliris et al. 2014; Tchilibou et al. 2015). This SPCZ fresh pool has a northwest–southeast orientation, extending from the WPWP toward French Polynesia (Gouriou and Delcroix 2002; Delcroix et al. 2011). Along the eastern edge of the SPCZ fresh pool, a surface ocean salinity front delineates its fresh waters from the high-salinity waters of the south-central Pacific Gyre (Fig. 1). The mean position of the salinity front is located near 15°–20°S, 175°W (Gouriou and Delcroix 2002). In

Corresponding author: Emilie P. Dassié, emilie.dassie@ird.fr

DOI: 10.1175/JCLI-D-17-0071.1

this study we use the 35.2-psu isohaline to identify the salinity front.

At interannual time scales, the SPCZ fresh pool mean position shifts with the phases of El Niño–Southern Oscillation (ENSO) (Gouriou and Delcroix 2002; Salinger et al. 1995, 2001, 2014). During El Niño events, the SPCZ fresh pool contracts toward a northeast position, and during La Niña events, it migrates to a more southwestern position (Vincent 1994; Salinger et al. 1995; Delcroix 1998; Gouriou and Delcroix 2002). At decadal time scales, the SPCZ fresh pool responds to the interdecadal Pacific oscillation (IPO; Power et al. 1999; see Newman et al. 2016 for a review) through both zonal and meridional movements along a northwest–southeast-oriented axis (e.g., Salinger et al. 2001; Folland et al. 2002; Linsley et al. 2006).

Studies of the long-term variations of the SPCZ fresh pool have been limited by the scarcity of observational SSS measurements. Recent studies have, however, shown a freshening of the fresh pool and its southeastward expansion since the 1970s (Cravatte et al. 2009; Singh et al. 2011; Delcroix et al. 2011). A modeling study indicates that this 30-yr long freshening trend is significantly different from what is expected from internal variability alone and suggests a discernible human influence (Terray et al. 2012). These recent decades of freshening are consistent with an intensifying global water cycle as the global climate system warms following the Clausius–Clapeyron relationship and the so-called wet-get-wetter and dry-get-drier paradigms (Held and Soden 2006; Chou et al. 2009; Durack et al. 2012; Skliris et al. 2014). SSS patterns in the western subtropical South Pacific result from a balance between surface forcing [evaporation minus precipitation ($E - P$)], horizontal water advection (at low and high frequencies), and subsurface forcing (entrainment and mixing; see Hasson et al. (2013) for a review]. Because of its influence on seawater density, SSS plays a key role in different atmosphere–ocean processes (Gouriou and Delcroix 2002; Cravatte et al. 2009; Terray et al. 2012; Hasson et al. 2013; Skliris et al. 2014; O'Kane et al. 2016). Investigating past SSS variability is therefore of great importance to infer possible changes in the hydrological cycle, water mass displacement and mixing, and variability of SSS frontal regions.

In tropical oceans, certain massive coral species can provide subannually resolved isotopic and geochemical records that accurately reflect seasonal, annual, and long-term changes in oceanographic conditions [e.g., sea surface temperature (SST) and SSS; see e.g., Linsley et al. 2006; DeLong et al. 2007; Dassié et al. 2014]. The Republic of Fiji (~16°S, 179°E), the Kingdom of Tonga (~20°S, 175°W), and the island of Rarotonga in the Cook Islands (~21.5°S, 159.5°W) (hereinafter FTR region) are located in a northwest–southeast transect perpendicular to the salinity front, providing unique locations to study the spatiotemporal variability of the SPCZ fresh pool (Fig. 1). Coral $\delta^{18}O$ is influenced by both SST and $\delta^{18}O$ of seawater ($\delta^{18}O_{sw}$), the latter being linearly related to SSS [see Corrège (2006) for a review]. Various studies from the FTR region have already reported that at interannual time scales, SSS is the primary driver of coral $\delta^{18}O$ variability in this region (Le Bec et al. 2000; Linsley et al. 2006, 2008; Dassié et al. 2014). Two individual coral records from Tonga and Rarotonga highlighted a progressive southeastward displacement of the SPCZ salinity front since the mid-1800s (Linsley et al. 2006). Superimposed on this secular trend, a strong multidecadal signal was also observed in Fiji and Tonga (Linsley et al. 2008; Dassié et al. 2014). Furthermore, these studies highlight the importance of water mass advection in the FTR region, despite being located in the heavy rainfall region of the SPCZ. A unique regional network of multiple coral records from Fiji (Dassié et al. 2014) validated that a multicoral local replication approach is preferred to assess the regional-scale climatic significance of coral-based geochemical time series reconstructions (Tudhope et al. 1995; Gagan et al. 1998; Guilderson and Schrag 1999; Linsley et al. 2015; Lough 2004; Stephans et al. 2004; DeLong et al. 2007). The present study builds on these aforementioned findings and adds a new coral record from Tonga, which allows application of the replication approach at all three sites in the FTR region. This will allow, for the first time, the constraining of the SPCZ salinity front variability, both temporally and spatially, by using robust coral composite records from all three sites in the FTR region. In this study we also assess the potential role of oceanic advection versus precipitation variability in the displacement of the SPCZ salinity front. After a brief presentation of the datasets and methods (section 2), we demonstrate that $\delta^{18}O$ from coral composite records allows deriving SSS variability in the FTR region. Based on these results, we document spatiotemporal variability of the fresh pool salinity front since the early 1880s at interannual, decadal, and secular time scales (section 3). The processes responsible for such variability are further explored by evaluating the potential role of surface forcing relative to other processes. Our results indicate the dominating influence of ocean circulation on SSS decadal variability and in the onset of the freshening trends.

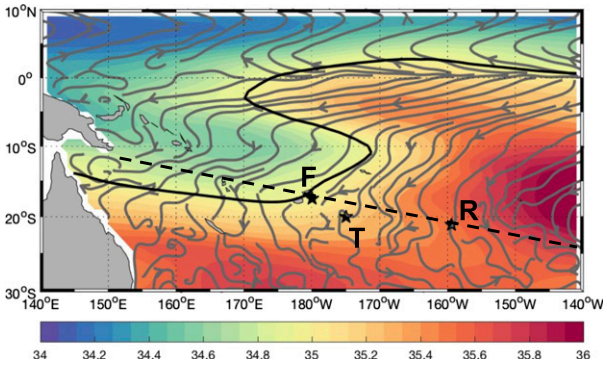

FIG. 1. Mean SSS (color shading; Delcroix et al. 2011) and streamlines of drifter-derived global near-surface currents (gray contours; Lumpkin and Johnson 2013) in the southwestern Pacific Ocean over the 1970–99 period. Stars indicate the three study sites [Fiji (F), Tonga (T), and Rarotonga (R)]. The black solid line represents the 35.2-psu isohaline characterizing the salinity front. (The dotted line corresponds to the transect used in Fig. 5.)

2. Materials and methods

a. Coral $\delta^{18}O$ data

Nine massive Porites coral cores are used in this study: four from Fiji, three from Tonga, and three from Rarotonga (Table 1). Correlation coefficients between individual coral $\delta^{18}O$ records are significant at the 99% confidence level (Table 2). In addition, standard deviations and variances (Table 3) are similar, implying a robust regional intercolony reproducibility. Following the approach presented in Dassié et al. (2014), coral composites for each site are created. Individual records from Fiji, Tonga, and Rarotonga are first centered by subtracting their respective 1960–90 $\delta^{18}O$ mean values, which is the time period common to all coral records. Coral composites were then created by averaging all records when at least two records per site exist. This study focuses on reconstructing interannual to longer time-scale variability; therefore, seasonal variability was removed by running a 25-month Hanning filter (Blackman and Tukey 1958) on every coral $\delta^{18}O$ series constituting the composites. More details of the individual coral records used in this study can be found in appendixes A and B. The methods used to build the age models (see Fig. A1) are described in appendix C.

b. Instrumental data

We use Delcroix et al. (2011) and the Simple Ocean Data Assimilation, version 2.2.4 (SODA2.2.4; Carton and Giese 2008), monthly SSS products, which both cover the FTR region and overlap with the most recent period of the coral data (1999). We selected grid boxes (1° resolution) in the Delcroix et al. (2011) SSS product (SSS_D) centered on 17°S, 179°E for Fiji; 20°S, 175°W for Tonga; and 21°S, 201°E for Rarotonga. We also sampled the SODA2.2.4 dataset (SSS_S) by selecting grid boxes (0.5° resolution) centered on 17.8°S, 179.8°E for Fiji; 20.3°S, 175.3°W for Tonga; and 21.3°S, 159.8°W for Rarotonga. After comparing the two products, we decided to only use SSS_D for our study as this dataset has a better coverage of the FTR region (see Figs. D1–D3, and appendix D for details).

Monthly sea surface temperature data from NOAA/NCDC Extended Reconstructed SST, version 4 (ERSST.v4; Smith et al. 2008), are also analyzed from grid boxes (2° resolution) centered on 18°S, 178°W for Fiji; 20°S, 176°W for Tonga; and 22 °S, 160°W for Rarotonga, going back to 1880.

Cumulative monthly precipitation records from various rain gauge sites around Fiji from January 1875 to July 2002 are retrieved from the Pacific rainfall (PACRAIN) database (http://pacrain.ou.edu/). Unfortunately, Tonga and Rarotonga do not have multiple observation sites on their islands to allow the creation of continuous rainfall time series. Comparison between PACRAIN and GPCP, version 2.2, datasets (Adler et al. 2003) in the Fiji area shows that both series are very similar and significantly correlated ($R = 0.70$, significant at the 99% confidence level) over the overlapping period (1979–2002). We therefore decided to use the PACRAIN product, as it goes further back in time, and only look at Fiji rainfall variability.

We rely on the objectively analyzed air–sea fluxes (OAFlux) from the WHOI OAFlux project (Yu 2007) to analyze the monthly mean evaporation changes starting in 1959. We averaged over six grid points (1° resolution) in the FTR region (16.5°S, 177.5°W; 17.5°S, 177.5°W; 16.5°S, 178.5°W; 17.5°S, 178.5°W; 16.5°S, 179.5°W; and 17.5°S, 179.5°W).

We used the sea level pressure (SLP) Southern Oscillation index (SOI) as an index of ENSO variability. A modern SOI index (SOI_Modern) and a historical SOI index (SOI_Historical) time series were extracted from the NOAA/Climate Prediction Center data repository (http://www.cpc.ncep.noaa.gov/data/indices/soi). Both SOI datasets are monthly time series of the standardized difference in sea level pressure between Tahiti and Darwin. The SOI_Modern time series is continuous from 1950 to 2016, while the SOI_Historical time series, going from 1882 to 1950, presents some gaps. When the succession of missing data is less than one year, missing months are filled with the mean value of the entire time series. For the period not covered by the SOI index, we used a 7-century-long ENSO reconstruction derived from tree rings (Li et al. 2013).

TABLE 1. Summary of the subseasonal resolution coral $\delta^{18}O$ time series. More details on TF1 can be found in appendix B.

Core	Species	Years[a]	Location	Lat, lon	Mean $\delta^{18}O$ value (‰)[b]	Publications
			Fiji			
1F	*Porites lutea*	1781–1997	Savusavu Bay, Fiji	16°49′S, 179°14′W	−5.14	Linsley et al., 2004
AB	*Porites lutea*	1617–2001	Savusavu Bay, Fiji	16°49′S, 179°14′W	−4.69	Linsley et al., 2006
FVB1	*Porites lutea*	1841–2004	Vanua Balavu, Fiji	17°20.1′S	−5.15	Dassié et al., 2014
16F	*Porites lutea*	1937–98	Aïwa Island, Fiji	18°19′S, 178°43′W	−4.80	Dassié et al. 2014
			Tonga			
TH1	*Porites lutea*	1944–2004	Ha'afera Island, Tonga	19°56′S, 174°43′W	−4.94	Linsley et al. 2008
TNI2	*Porites lutea*	1848–2004	Nomuka Island, Tonga	20°16′S, 174°49′W	−4.73	Linsley et al. 2008
TF1	*Porites lutea*	1883–2004	Fonoifua Island, Tonga	20°16′S, 174°38′W	−4.72	This study
			Rarotonga			
2R	*Porites lutea*	1726–1996	Rarotonga, Cook Islands	21°14′S, 159°49′W	−4.45	Linsley et al. 2000, 2004
3R	*Porites lutea*	1874–2000	Rarotonga, Cook Islands	21°14′S, 159°49′W	−4.38	Linsley et al. 2004
99	*Porites lutea*	1906–99	Rarotonga, Cook Islands	21°14′S, 159°49′W	−4.54	Linsley et al. 2004

[a] Years where millimeter-scale resolution is available.
[b] For the common time period of all the cores (1944–96).

This tree-ring index (labeled ENSO tree-ring index) is based on 2222 tree-ring chronologies from both the tropics and midlatitudes in both hemispheres. We also used a new index of the position of the SPCZ (SPCZI) developed by Salinger et al. (2014). This index is based on quality-controlled and recently homogenized mean sea level pressure records for the South Pacific during the austral warm season (November–April) covering the 1910/11–2011/12 period.

c. *Trend analyses and statistical testing*

Pearson product moment correlation coefficients (referred to as correlation) are used to determine the significance of relationships. If not specified, the significance is calculated at the 99% confidence level. The degree of freedom (df) was adjusted for autocorrelation using Draper and Smith (1998) test runs.

The frequency components of the coral $\delta^{18}O$ composites were determined via a red-noise spectral analysis [REDFIT from the Paleontological Statistics (PAST) software package for education; Hammer et al. 2001]. The variability of the frequency distribution through time is obtained using wavelet analyses (wavelet transform from R package biwavelet; Torrence and Compo 1998; Liu et al. 2007).

To extract the long-term trend, we fit a polynomial function to the coral $\delta^{18}O$ composites time series. To determine the break points in trends, we looked at robust changes in the mean-square error of the time series' first derivative (Bai 1994).

To remove seasonal variability and highlight interannual to long-term variability, we used a 25-month Hanning filter (Blackman and Tukey 1958). Interannual mode of variability is extracted by removing the long-term

TABLE 2. Correlation matrices between individual records for each site over their common time period (1945–97). All values are significant at the 99% confidence level. The left part of the matrix corresponds to monthly data and the right part to interannual data (Hanning-filtered data).

		Interannual time scale–Hanning-filtered data									
		Fiji				Tonga			Rarotonga		
		1F	AB	FVB1	16F	TH1	TNI2	TF1	2R	3R	99
Fiji	1F	—	0.53	0.47	0.46						
	AB	0.70	—	0.53	0.53						
	FVB1	0.62	0.63	—	0.85						
	16F	0.63	0.74	0.83	—						
Tonga	TH1					—	0.83	0.64			
	TNI2					0.80	—	0.58			
	TF1					0.62	0.75	—			
Rarotonga	2R								—	0.75	0.70
	3R								0.79	—	0.65
	99								0.80	0.80	—

TABLE 3. Standard deviation and variance (‰) of the individual records over their common time period (1945–97) for both monthly and Hanning-filtered data.

	Fiji				Tonga			Rarotonga		
	1F	AB	FVB1	16F	TH1	TNI2	TF1	2R	3R	99
					Seasonal time scale					
Std dev	0.23	0.23	0.22	0.23	0.22	0.24	0.25	0.20	0.24	0.23
Variance	0.053	0.053	0.049	0.051	0.048	0.057	0.061	0.040	0.059	0.052
					Interannual time scale–Hanning-filtered data					
	1F	AB	FVB1	16F	TH1	TNI2	TF1	2R	3R	99
Std dev	0.11	0.11	0.13	0.13	0.09	0.08	0.11	0.10	0.10	0.09
Variance	0.011	0.012	0.017	0.017	0.007	0.007	0.013	0.010	0.011	0.007

trend from the time series. The residual is then centered and normalized by removing its mean and dividing by its standard deviation.

d. *Linear modeling approach to infer coral-based SSS data*

The assessment of the coinfluence of SST and SSS on coral δ^{18}O time series indicates that at interannual time scale, SSS variability is the leading factor of coral δ^{18}O variability (see appendix E for details). To investigate the percentage of SSS variance explained by interannual δ^{18}O time series and determine its validity to reconstruct past SSS variability, we use a statistical linear modeling approach. Linear regressions were made between Fiji, Tonga, and Rarotonga coral δ^{18}O composites and SSS_D. Different calibration and reconstruction periods are tested to infer the robustness of the model: (i) the entire length of the instrumental record (1970–2000), (ii) 1970–85, and (iii) 1985–2000 (Fig. E1 and Table E1).

At Fiji, the SSS_D variance explained by the coral δ^{18}O is about 80% for all three periods (87% for 1970–85; 72% for 1985–2000; and 79% for 1971–2000). At Fiji, coral δ^{18}O-based SSS reconstructions are not influenced by the calibration periods used. At Tonga, the percentage of explained variance ranges from 52% to 68% depending on the period considered (68% for 1970–85; 52% for 1985–2000; and 56% for 1971–2000). The calibration period for the Tonga record does not however have a large impact on the reconstruction, in spite of the 1970–85 calibration period having a tendency to increase the amplitude of the signal. For Rarotonga, the percentage of explained variance is also not similar among the periods, with 39%, 44%, and 55% for the 1970–2000, 1970–85, and 1985–2000 periods, respectively. The choice of the calibration period does have a large impact on the reconstruction at the Rarotonga site. The 1985–2000 calibration period has a tendency to increase the reconstruction signal amplitude as well as the low-frequency variability. Strong ENSO events such as the 1988/89 La Niña and the 1997/98 El Niño lead to higher than usual interannual variability, which may be responsible for the reconstruction bias seen when using the 1985–2000 calibration period. The lower percentage of explained SSS variance at Rarotonga compared to other sites might be related to the weaker robustness of the instrumental SSS data. The number of observations per year used to create the instrumental time series at Rarotonga is indeed lower than at both Fiji and Tonga (see appendix D).

At frequencies lower than interannual time scales, secular variability of SST and SSS are also not independent (see appendix E for more details). We therefore cannot remove the SST influence on the long-term δ^{18}O trend. We decided to focus only on δ^{18}O-derived SSS (coral SSS) for the rest of this study.

e. *Methodology to quantify the influence of precipitation on SSS variability*

Hasson et al. (2013) assessed the mechanisms affecting the mixed layer salinity (MLS) in the tropical Pacific Ocean over the 1990–2009 period. They described the salinity budget as a sum of horizontal advection, surface, and subsurface forcings. In this section we focus on the influence of the precipitation term on SSS variability as described by (term II of Hasson et al. 2013):

$$\partial_t S = \frac{(E-P)}{H} S. \quad (1)$$

The left-hand side of the equation is the temporal salinity variability represented by the first derivative of the monthly coral SSS time series. The right part of the equation represents the SSS variability in response solely to surface forcing variability. To isolate the influence of precipitation, we had to set all the other terms in Eq. (1). The mixed layer depth H was fixed to 35 m, following the mean annual climatology presented by de Boyer Montégut et al. (2004). For the salinity S, we used

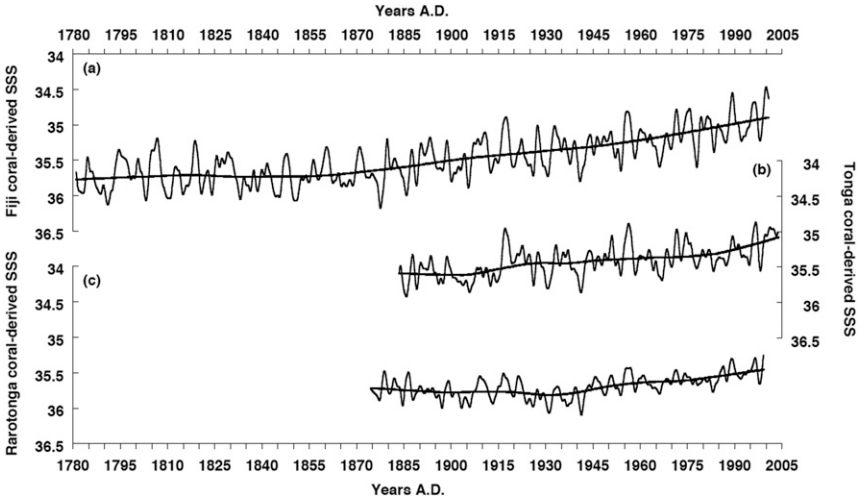

FIG. 2. Coral-derived SSS time series from (a) Fiji, (b) Tonga, and (c) Rarotonga, filtered with a 25-month Hanning filter (thin black lines), and their long-term trend (thick line). The thick line was obtained by fitting a polynomial function to the time series.

the monthly coral SSS time series, assuming that it represents the average salinity of the mixed layer. For the precipitation P and evaporation E, we used the PACRAIN and the OAFlux databases, respectively (section 2b). For the period preceding 1959, for which we do not have evaporation data, we determined the OAFlux mean values over the 1959–99 period, which give an average value of $1.77\,\mathrm{m\,yr^{-1}}$. This value is consistent with observations in the FTR region made by Yu (2011). We feel confident in presuming a constant E value since (i) evaporation does not present any significant long-term variation over the 1979–2008 period (see Terray et al. 2012, their Fig. 2a), (ii) the contribution of the evaporation component in the $E - P$ ratio is small in precipitation-dominated areas (Delcroix et al. 2007; Yu 2011), and (iii) the mean difference between both SSS variability inferred from precipitation using a constant E and OAFlux E values is small (0.01) and not significant (at the 99% confidence level). To focus on interannual variability, both coral SSS (SSS_Coral) and SSS variations inferred from precipitation (SSS_Precipitation) are filtered with a 25-month Hanning filter.

3. Results

a. Coral-based SSS time series

Fiji, Tonga, and Rarotonga coral SSS time series are shown in Fig. 2. The series present similar variability spectra, a secular trend, and higher frequency modes. Over the common period (1883–1999), intersite correlations are 0.84 for Fiji and Tonga, 0.75 for Fiji and Rarotonga, and 0.66 for Tonga and Rarotonga, all significant at the 99% confidence level. Spectral analyses indicate occurrences of frequency peaks consistent with ENSO (Figs. 3a–c), which, however, decrease in amplitude from Fiji to Rarotonga. Decadal spectral peaks are evident but are below the 99% confidence level. Wavelet analyses (Figs. 3d–f) over the entire length of each record (1781–2000 for Fiji, 1883–2003 for Tonga, and 1874–1999 for Rarotonga) further reveal power in the entire ENSO spectral band (from 2 to 8 yr), significant throughout the records. At Rarotonga a decadal mode above 10 and below 16 yr is present, but is significant only after 1900.

b. Coral-based SSS interannual variability

Coral-derived SSS anomalies at Fiji, Tonga, and Rarotonga are shown in Fig. 4 and compared to the SOI, the ENSO tree-ring index, and the SPCZ index (see Table 4). For each site, a significant negative correlation is found with the SOI (see Table 4). When considering the entire 1883–1999 SOI time series (including both SOI_Modern and SOI_Historical), correlation values are still significant but much weaker, highlighting increased uncertainties introduced when considering the SOI_Historical index before the 1950s. Correlation with the ENSO tree-ring index over the 1883–1999 period also gives significant but weaker values as compared to when only considering the 1950–99 recent period. Interestingly, coral SSS are positively correlated with the SPCZI over the 1910–99 period (Table 4), confirming the relevance of our selected sites to capture past SPCZ position interannual variability in response to ENSO (Salinger et al. 2014).

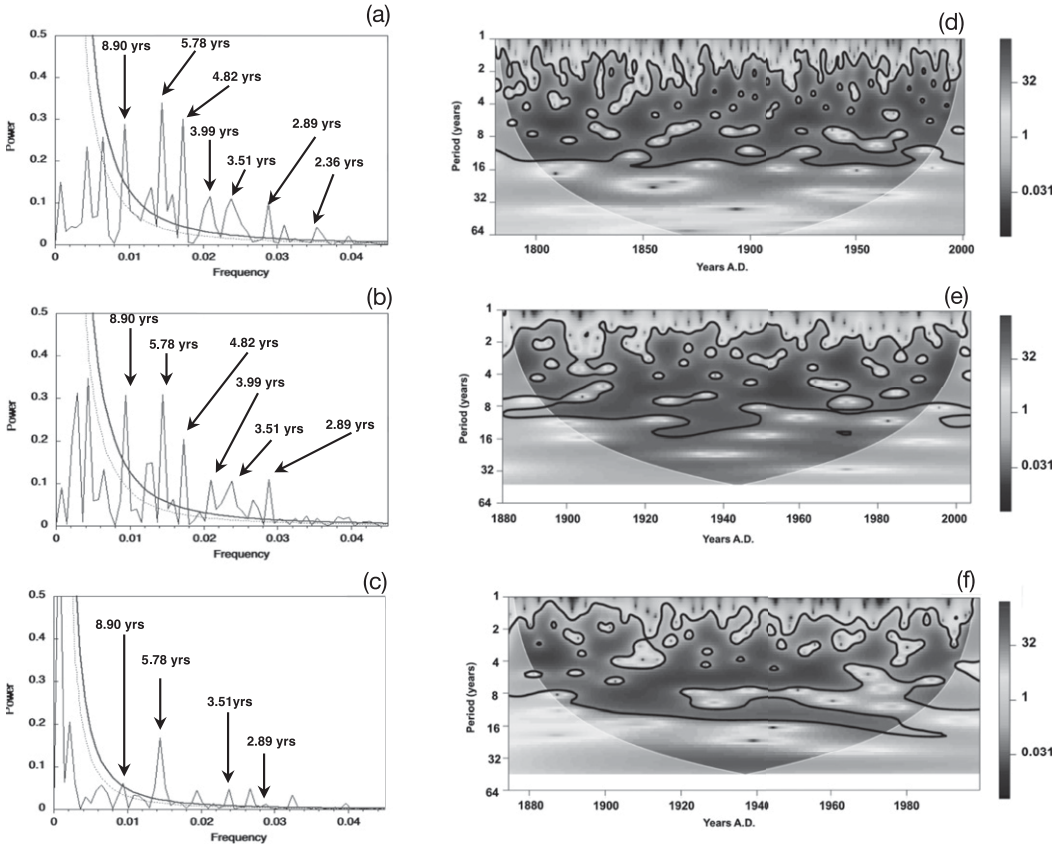

FIG. 3. REDFIT spectral analysis of coral-derived SSS time series (Hammer et al. 2001) at (a) Fiji, (b) Tonga, and (c) Rarotonga over the 1883–1999 period. The 99% and 95% confidence levels of statistical significance are indicated by the solid and dotted black curves, respectively. Morlet wavelet analyses of coral-derived SSS time series at (d) Fiji, (e) Tonga, and (f) Rarotonga are shown for the entire length of each record: 1781–2000 for Fiji, 1883–2003 for Tonga, and 1874–1999 for Rarotonga. The thick black contours in (d)–(f) indicate the 99% confidence level of statistical significance.

Over the 1950–2000 instrumental period, all major ENSO events (eight El Niño and seven La Niña events) are detected when coral SSS anomalies exceed a 0.75 standard deviation threshold in our coral-based records (Fig. 4). Over the 1883–1950 period, we further identify seven El Niño and six La Niña events in our records for the FTR region. El Niño and La Niña events for the pre-1950 period are not easily identified in the SOI_ Historical time series since many years are missing in the record.

Coral SSS at Fiji, Tonga, and Rarotonga also show spatial variability of the SPCZ fresh pool through time (Fig. 5). Over the instrumental period, the SSS zonal gradient seen in instrumental SSS data is well represented by coral-based SSS data (Fig. 5a). We can therefore use coral-based SSS data to reconstruct past displacements of the salinity front. Linear regressions were made between the longitudinal position of the 35.2-psu isohaline and coral SSS normalized anomaly time series at Fiji, Tonga, and Rarotonga over the 1970–99 period (Table 5). Fiji, Tonga, and Rarotonga interannual coral SSS variability explain 75%, 37%, and 49% of the longitudinal position of the salinity front variance, respectively. Using the three sites as a predictor increases the explained variance to 80%, which is, however, not significantly different from the explained variance obtained when using the Fiji SSS time series only (dark and light gray lines in Figs. 5a,b). Predictions of the 35.2-psu isohaline position from Fiji and FTR region are highly correlated over the instrumental time period (1970–99; $R = 0.97$, significant at the 99% confidence level) as well as over the overlapping period (1883–99; $R = 0.96$, significant at the 99% confidence level). These significant correlations imply that a large portion of the salinity front displacement is influenced by SSS variability around Fiji. Interannual displacements of the salinity front are observable over the last 200 years; however, no changes in amplitude are detected.

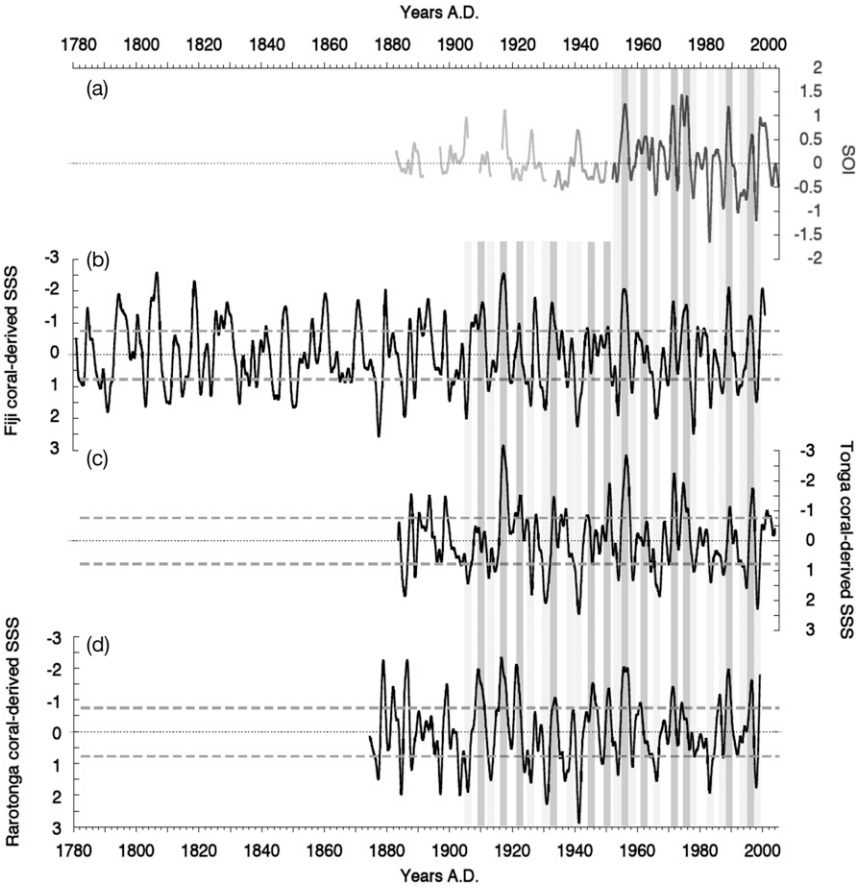

FIG. 4. (a) SOI_Modern (1950–2016, black curve) and SOI_Historical (1882–1950, light gray curve) time series and (b) Fiji coral-derived SSS (black curve). (c),(d) As in (b), but at Tonga and Rarotonga, respectively. The FTR-region series were first filtered with a 25-month Hanning filter, detrended, and standardized. Dotted horizontal lines in (b)–(d) indicate the 0.75 standard deviation threshold that we define to detect ENSO events. The dark and light gray vertical shading indicates El Niño and La Niña years, respectively. Note that in (b)–(d), the *y* axis is reversed.

c. *Coral-based SSS secular variability*

The long-term trend in coral SSS time series reveals a significant freshening trend (Figs. 2 and 5c), the onset of which varies from one site to another (Table 6). At Fiji, SSS is relatively stable until around 1865 when a significant near-linear freshening is detected of about −0.06 psu decade^{-1}. A similar trend appears at Rarotonga around 1939, with a significant linear freshening of −0.047 psu decade^{-1}. At Tonga, the coral SSS record also indicates a significant freshening trend but it is much weaker, of about −0.012 psu decade^{-1}, and appears much later, around 1982.

d. *Influence of precipitation on SSS variability*

Interannual SSS_Coral and SSS_Precipitation (see section 2e) are presented in Fig. 6a. Despite an overall similar variance, the correlation between SSS_Coral and SSS_Precipitation is not significant when considering the entire length of the records. Over decadal time scales however, periods with correlation values higher/lower than ±0.5 are detected with nine periods with a

TABLE 4. Correlation coefficients between the FTR-region monthly coral-derived SSS anomalies time series and the SOI (SOI_Modern: 1950–99; SOI_Modern and SOI_Historical: 1882–1999). Correlation coefficients between the FTR-region annual-averaged coral-derived SSS anomalies time series and ENSO tree-ring index (Li et al. 2013: 1883–1999) and the SPCZI (Salinger et al. 2014: 1911–99). All the values are significant at the 99% confidence level.

	Fiji	Tonga	Rarotonga
SOI_Modern	−0.70	−0.65	−0.67
SOI_Modern and SOI_Historical	−0.38	−0.35	−0.33
ENSO tree-ring index	−0.48	−0.55	−0.35
SPCZI	0.48	0.58	0.43

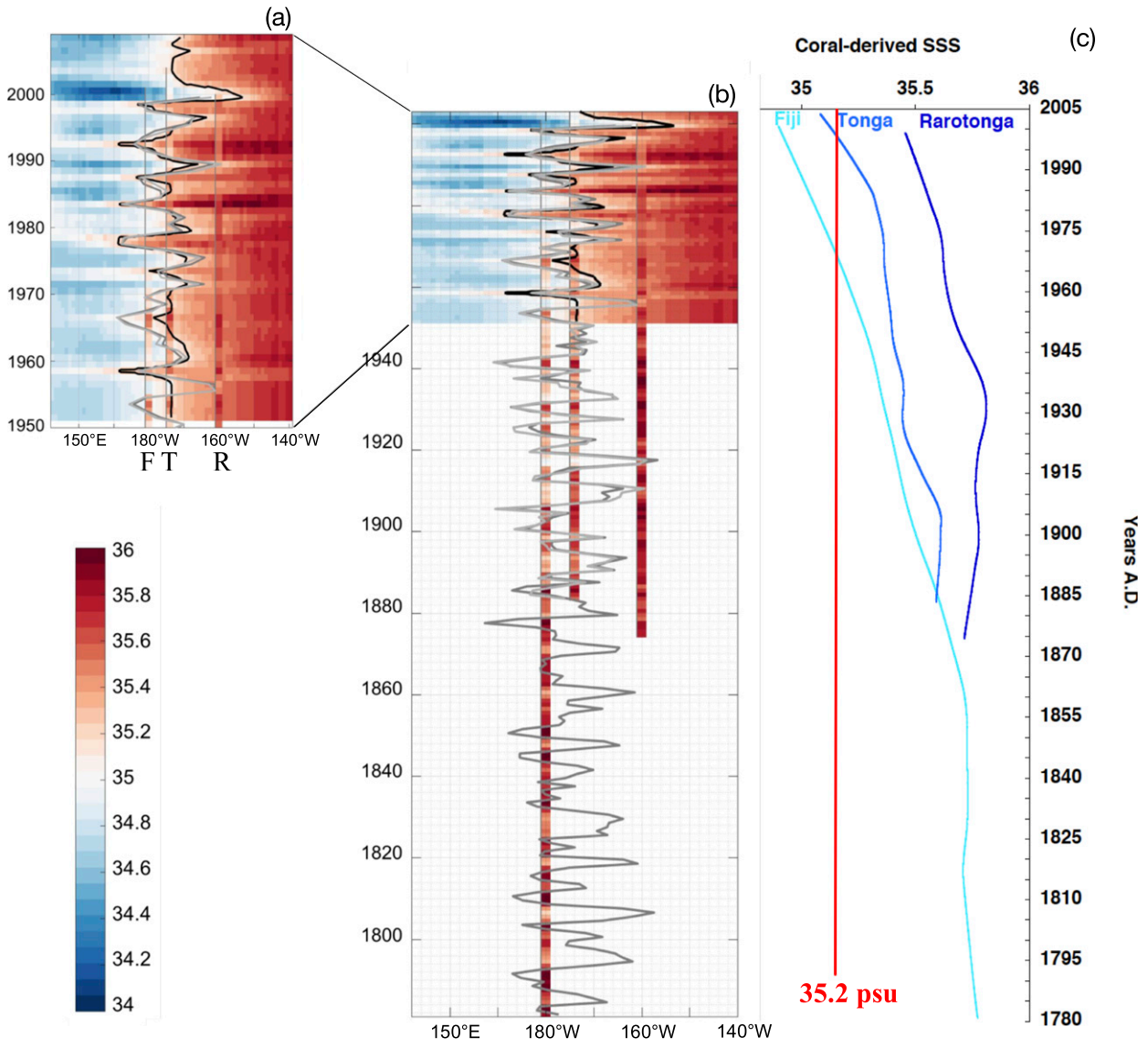

FIG. 5. (a) Hovmöller diagrams of SSS along a northwest–southeast transect (dotted line in Fig. 1) in the southwestern Pacific Ocean from 1950 to 2005. On top of instrumental SSS anomalies (background color shading; Delcroix et al. 2011), the coral-derived SSS anomalies are inserted at their respective longitudes corresponding to Fiji (F), Tonga (T), and Rarotonga (R) (see Fig. 1). The black line indicates the instrumental 35.2-psu isohaline longitudinal position. The prediction of the 35.2-psu isohaline position using coral-based SSS time series from Fiji only is shown (dark gray line) together with the prediction obtained using Fiji, Tonga, and Rarotonga time series (light gray line). (b) As in (a), but from 1870 to 2005. (c) Long-term trend of the coral-derived SSS data from Fiji (light blue), Tonga (medium blue), and Rarotonga (dark blue).

significant positive correlation (at least at the 90% confidence level) and three periods with a negative correlation (significant at the 90% confidence level; Fig. 6b). These periods do not correspond to any specific ENSO events. Over longer time scales, the 30-yr-window rolling correlation (Fig. 6c) reveals a consistent pattern of correlation, with periods of persistent positive (1890–1905, 1915–28, and 1945–72), negative (1928–45), and weakly negative (1905–15 and 1972–85) correlations. Interestingly, despite not being significant, positive and negative correlation phases correspond to negative and positive IPO phases, respectively. These results are consistent with previous work showing coherent multidecadal variability in the SPCZ and IPO signals (Salinger et al. 2001; Folland et al. 2002) and more recent studies using historical rainfall datasets (Lorrey et al. 2012; Salinger et al. 2014). Our results confirm that during negative IPO phases, when

TABLE 5. Linear regression model fraction of variance explained R^2, slopes, and intercept obtained between the longitudinal position of the 35.2-psu isohaline and FTR-region coral-derived SSS normalized anomaly time series over the 1970–99 period. All the values are significant at the 99% confidence level except those in italics.

	R^2	Slope	Intercept
Lon vs Fiji	0.75	−7.59 ± 0.84	184.68 ± 0.78
Lon vs Tonga	0.37	−5.96 ± 1.46	185.16 ± 1.23
Lon vs Rarotonga	0.49	−6.57 ± 1.26	184.45 ± 1.11
Lon vs			
FTR region	0.8	—	184.38 ± 0.73
Fiji	—	−8.28 ± 1.46	—
Tonga	—	*2.87 ± 1.49*	—
Rarotonga	—	*−2.19 ± 1.16*	—

the SPCZ is over the FTR region, the associated precipitation signal drives the SSS signal, which is not the case during a positive IPO. To decipher the level of influence of precipitation on the SSS signal, we derived the residual SSS by removing precipitation-induced SSS variations (Fig. 6d). The 30-yr-window rolling correlation between coral SSS and residual SSS is positive all the way though the record with significant correlations (at least at the 90% confidence level) during positive IPO phases and the oldest negative IPO phase. This indicates that SSS variability in the FTR region is influenced by factors other than precipitation.

4. Discussion

a. Interannual variability

Fiji, Tonga, and Rarotonga coral SSS signals show significant coherent variability at interannual time scales (Fig. 3). Significant correlations between coral-based SSS detrended time series and the SOI, the ENSO tree-ring index, and the SPCZI (Fig. 4 and section 3b) suggest that salinity front displacements in the FTR region are strongly influenced by ENSO.

Recent studies have shown an increase in both ENSO variance (e.g., Li et al. 2013) and occurrences of extreme ENSO events (e.g., Cai et al. 2012) over the last 30 years. Our dataset, however, does not provide evidence of any significant changes in ENSO event frequency when put within a longer-term perspective. The number of detected ENSO events in our records for the FTR regiondid not significantly change before and after 1950 (eight El Niño and six La Niña events during the 1950–99 period and six El Niño and six La Niña events during the 1900–50 period). Additionally, 30-yr running variance (not presented here) of Fiji, Tonga, and Rarotonga detrended coral-based SSS time series do not present any significant changes over the 1883–1999 period. ENSO-induced precipitation in remote areas and therefore SSS interannual variability over the southwestern Pacific might respond differently from ENSO-induced SSS variability in the equatorial Pacific band such as presented by Cai et al. (2012).

Besides changes in ENSO variance, studies have pointed out that different El Niño events may have very different signatures in the southwestern Pacific region. Vincent et al. (2011) indicates that some asymmetric El Niño events (1982/83, 1991–93, and 1997/98) correspond to a strong northeastward shift of the SPCZ rainfall axis. Using SSS observations, Singh et al. (2011) looked at the contrasting SSS features in the tropical Pacific during central Pacific (CP: 1977/78, 1986–88, 1990/91, and 1992–95) and eastern Pacific (EP: 1982/83, 1991/92, and 1997/98) ENSO events. They demonstrated that during EP El Niño events [same events as Vincent et al. (2011)'s asymmetric events], the SPCZ region is characterized by a marked increase in SSS, which is about 2–3 times more than during CP El Niño events. Therefore, we expect to see different SSS signals at our sites in the FTR region, depending on the flavor of ENSO events. The 1982/83 and 1997/98 CP El Niño events present a large increase in SSS at all three sites, but not the 1991–93 event (Fig. 4). Looking at the position of the salinity front during the three EP El Niño events, the FTR-region reconstructed salinity front (Fig. 5a) is located west of Fiji. Nevertheless, the 1977/78 CP El Niño event resulted in a larger displacement. We looked at EP La Niña events (1985/86, 1988/89, 1995/96, and 1999–2001) compared to the 1983/84 and 1998/99 CP

TABLE 6. Trends (decade^{-1}) for different time periods from FTR-region coral-derived δ^{18}O-SSS, $\delta^{18}O_{sw}$-SSS, and instrumental SST (ERSST.v4; Smith et al. 2008) and break points, determined using the mean-square error of the time series' first derivative.

	Fiji		Tonga		Rarotonga	
	Break point	Slope	Break point	Slope	Break point	Slope
δ^{18}O-SSS	1865	−0.056 psu (1865–2000)	1982	−0.012 psu (1982–2003)	1939	−0.047 psu (1939–99)
SST	1914	+0.028°C (1914–99)	1914	+0.017°C (1914–99)	1914	+0.033°C (1914–99)
δ^{18}O-SSS	—	−0.062 psu (1914–99)	—	−0.033 psu (1914–99)	—	−0.042 psu (1914–99)
$\delta^{18}O_{sw}$-SSS	—	−0.054 psu (1914–99)	—	−0.017 psu (1914–99)	—	−0.031 psu (1914–99)

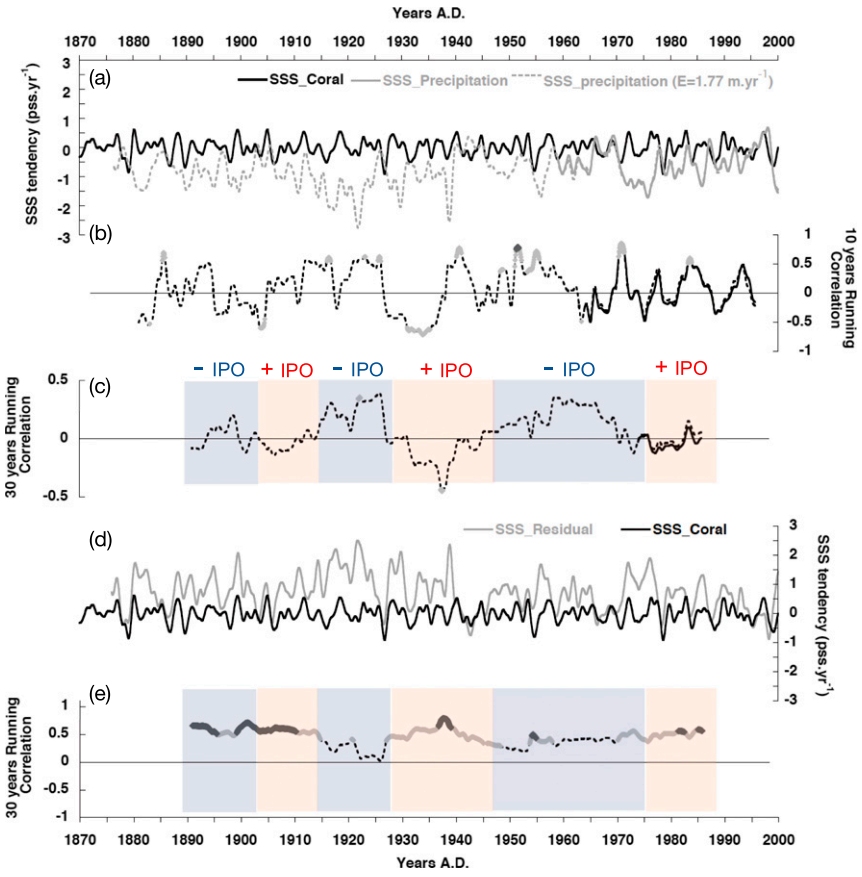

FIG. 6. (a) Fiji SSS_Coral first derivative monthly time series [black curve; left-hand side of Eq. (1)] and SSS_Precipitation [right-hand side of Eq. (1)], using instrumental evaporation time series (gray curve) or a mean value of 1.77 m yr^{-1} (dotted gray curve). (b) Correlation between coral-derived SSS and precipitation-derived SSS using a 10-yr running window. (c) As in (b), but with a 30-yr running window. (d) SSS residual obtained by removing precipitation-induced SSS variations from the coral-derived SSS first derivative. (e) Correlation between coral-derived SSS and SSS residual using a 30-yr running window. Light gray and dark gray dots in (b),(c),(e) indicate a significant correlation at the 90% and 99% confidence level, respectively. Blue and red shading in (c),(e) highlight periods with negative and positive IPO phases, respectively.

La Niña events. The last three EP La Niña events resulted in a larger SSS decrease at the three sites than the two CP La Niña events (Fig. 4). This is confirmed by the position of the reconstructed salinity front (Fig. 5a). During EP La Niña events, the salinity front moves close to Rarotonga (except for the 1985/86 event). The salinity front is located between Tonga and Rarotonga for both CP La Niña events. For the majority of ENSO events, the amplitude of the interannual FTR-region reconstructed SSS variability resembles that observed by Singh et al. (2011). The amplitude of FTR-region SSS variability could therefore be used to reconstruct past occurrences of both CP and EP events back to 1883. Combining ocean model reanalysis and a more extensive coral SSS dataset covering both the equatorial Pacific and the SPCZ mean area will better constrain past EP versus CP ENSO events. This is, however, outside the scope of this study.

The position of the SPCZ thus influences SSS variability in the southwestern Pacific, but precipitation cannot explain all SSS interannual anomalies. The lack of significant correlation between coral SSS and SSS variations inferred from precipitation (Fig. 6a) and the significant correlation between SSS and SSS residual especially during positive IPO phase (Figs. 6d,e) indicate that other factors are influencing interannual SSS variability in the FTR region. The SSS residual might be representative of anomalies in the zonal geostrophic advection component of surface ocean currents in the SPCZ region. Over the instrumental period (1976–2000), the SSS front displacement is correlated with the

SOI, and during the 1987/88 and 1997/98 El Niño events for example, westward and slightly northward surface geostrophic current anomalies were observed (Gouriou and Delcroix 2002). These current anomalies reverse during La Niña, with eastward current anomalies in phase with southeastward displacement of the fresh pool (Singh et al. 2011; Hasson et al. 2013). Our results are therefore consistent with observations and suggest a dominant influence of the South Equatorial Current (SEC), the main zonal current in our region of interest, as well as the South Pacific Gyre strength in the east–west movement of the SSS front on interannual time scale at least since the early 1880s.

b. *Decadal-scale variability and trends*

Our reconstructed coral-based SSS time series from Fiji, Tonga, and Rarotonga enable us to put into perspective the freshening trend observed since 1970 (Cravatte et al. 2009). Our records show that the observed eastward displacement of the salinity front is part of a longer-term trend that started before the 1970s, as already suggested by Linsley et al. (2006). The salinity front, defined by the 35.2-psu isohaline, migrated from west of Fiji to between Fiji and Tonga as early as 1865 in our records (Fig. 5c and Table 6). Since interannual coral SSS variance, mainly driven by the natural ENSO mode of variability, does not present any trend, the secular freshening is therefore unlikely due to internal climate variability. This is in agreement with Terray et al. (2012) who concluded, using instrumental tropical Pacific SSS data combined with climate model simulations, that the western Pacific freshening trend was not consistent with internal climate variability, and suggested a discernible human influence. Two hypotheses can be formulated to explain this secular freshening trend: 1) a progressive eastward displacement and/or intensification of the SPCZ rainfall axis, and/or 2) changes in ocean circulation, such as relaxation of the SEC or its southward shift related to basin-scale wind stress and gyre dynamics (see Hill et al. 2011).

Based on the normalized mean sea level pressure difference between Suva (Fiji) and Apia (Samoa), Salinger et al. (2014) concluded there was little overall change in the mean northeast–southwestern position of the SPCZ back to 1910. The long-term freshening trend observed at the three sites cannot therefore be only due to a progressive displacement of the SPCZ. An increase in atmospheric freshwater flux, following the wet-get-wetter paradigm (see Held and Soden 2006), can lead to a decrease in SSS over the FTR region. Fiji instrumental precipitation data from the PACRAIN database does not show a significant long-term trend over the 1875–2002 period. A trend in freshwater flux increase is therefore unlikely to be responsible for such an observed SSS decrease trend.

The 30-yr-window running correlation between coral SSS and SSS variations inferred from precipitation (Fig. 6c) highlighted periods of positive and negative correlations. These phase switches, despite not being significant, are synchronous with changes in IPO phases (Salinger et al. 2001; Folland et al. 2002; Fig. 6c). During negative (positive) IPO phases, the SPCZ tends to move southwest (northeast), which results in above (below) average precipitation over the Fiji area. For the period covered by instrumental SSS records (1970 onward), studies have shown that multidecadal variability exerted a substantial control over the spatial pattern of precipitation and SSS in the tropical Pacific Ocean (Delcroix et al. 2007; Skliris et al. 2014). Over the last 120 years, despite showing some IPO-related precipitation influence mostly during the negative phase, our results suggest the effect of another factor controlling Fiji SSS variability (Fig. 6c). This result is in line with the combined observations and modeling results of Terray et al. (2012) over the late twentieth century. They showed that SSS changes exhibit a much larger spatial-scale pattern than the freshwater fluxes, suggesting the influence of other factors, such as ocean circulation, in spreading the freshwater anomaly. In view of the Terray et al. (2012) conclusions and the lack of significant correlation between SSS_Coral and SSS_Precipitation (Fig. 6c) especially during the positive IPO phase, we presume that other factors, such as an intensification and relaxation of the SEC, might play a significant role in the secular freshening trend seen in the FTR region.

The Southwest Pacific Ocean Circulation and Climate Experiment (SPICE; Ganachaud et al. 2014) indicated that the southwestern Pacific Ocean is the center of major water pathways from the subtropics to the equator and to southern latitudes. Transports are large and vary substantially depending on time scales (Ganachaud et al. 2014). Additionally, large water volume transport occurs in narrow jets close to coastlines and reefs and is not well sampled (Kessler and Cravatte 2013). Those aforementioned studies focused on the Coral Sea region northwest of the FTR region; however, similar conclusions can certainly be drawn from our area, especially regarding the large-scale turbulent pathways of near-surface currents, which are already observable on their climatology (Fig. 1).

The onset of the freshening varies from site to site (Fig. 5c; Table 6), with Fiji leading with a break in trend around 1865, followed by Rarotonga around 1939, and

Tonga in the early 1980s. The lack of consistency in the timing of the trend's start across the FTR-region transect might corroborate the influences of ocean dynamics and its nonhomogenous pattern across the FTR region.

5. Summary and conclusions

This study evaluates the use of Fiji, Tonga, and Rarotonga coral composite $\delta^{18}O$ as a suitable proxy for past SSS variability in the southwestern Pacific. With 79%, 56%, and 39% of SSS variance captured by coral $\delta^{18}O$ composites at Fiji, Tonga, and Rarotonga, respectively, we created linear models to reconstruct FTR-region coral SSS variability back to the early 1880s. This allows the generation of a longer-term perspective on interannual and longer-term SPCZ fresh pool variability.

At the interannual time scale, the displacement of the salinity front is strongly modulated by ENSO events. The different flavors of ENSO as described in recent studies (e.g., Singh et al. 2011) are observable in the amplitude of the salinity front interannual displacement. However, combining ocean model reanalysis and a more extensive coral SSS dataset covering both the equatorial Pacific and the SPCZ mean area is needed to obtain a more robust index of past EP versus CP ENSO. While some studies found an increase in both the amplitude and the frequency of ENSO over recent decades (Cai et al. 2012; Li et al. 2013) our records show no evidence of such changes since the early 1880s. The lack of significant correlation between interannual SSS variability and precipitation-induced SSS changes in the FTR region imply the role of another factor, such as ocean advection on interannual SSS variability.

Over the last 200 years, our study reconstructs an eastward displacement of the salinity front. This result puts into perspective the last 30 years of freshening observed in the instrumental data, which might provide a benchmark for testing the coupled climate models' ability to represent SPCZ fresh pool trends. On this time scale, precipitation variability seems not to be the leading factor, indicating that ocean dynamics have been playing a significant role in the long-term freshening trend in the FTR region.

Acknowledgments. We thank the three anonymous reviewers for their constructive comments on earlier versions of this contribution. B. K. Linsley thanks the governments of Rarotonga (Cook Islands), Fiji (Ministry of Fisheries and Forests), and the Kingdom of Tonga (Ministry of Fisheries in Nuku'alofa) for supporting the field phases of this research. He also thanks the following people and organizations for their assistance over the many phases of this project: S. Tuilaucala (Director of Fisheries) and A. Batibasaga (Principal Research Officer) of the Government of Fiji (Ministry of Fisheries and Forests); 'Ulunga Fa'anunu (Acting Secretary of Fisheries, Tonga); G. M. Wellington; O. Hoegh-Guldberg; J. Caselle; D. Mucciarone; T. Potts; S. Bagnato; S. Kafka; G. Brosnan (Broz); K. McGrath; A. Paulin; A. Stolorow; S. Tudhope; P. B. de Menocal; and the J. M. Cousteau Resort (Fiji). The U.S. National Science Foundation and U.S. National Oceanic and Atmospheric Administration provided funding to B.K. Linsley to collect the corals and generate the geochemical results discussed here (NSF Grants ATM-9901649 and OCE-0318296 and NOAA Grant NA96GP0406). Dr. Linsley's participation in this specific contribution was partially supported by the Vetlesen Foundation via a gift to the Lamont-Doherty Earth Observatory.

APPENDIX A

Individual Coral Records and the Creation of Coral Composites

The 10 coral records from Fiji, Tonga, and Rarotonga used in this study were collected during expeditions that took place in 1997, 1999, 2000, and 2004. Descriptions of the Fiji coral cores 1F and AB are given by Linsley et al. (2004, 2006) and Fiji coral cores FVB1 and 16F were presented by Dassié et al. (2014). Description of Tonga cores designated TH1 and TNI2 can be found in Linsley et al. (2008). A new coral record from Tonga (TF1) is added in this study and described in appendix B. Coral core TM1, originally discussed in Linsley et al. (2008), is not included in this study because of the subsequent realization that a coral fungal infection had influenced skeletal $\delta^{18}O$ (Linsley et al. 2008; B. K. Linsley 2010, unpublished results). Descriptions of Rarotonga coral cores (2R, 3R, and 99) are presented in Linsley et al. (2000, 2004) and Ren et al. (2003). Only coral cores sampled at a millimeter-scale resolution were used; this resolution (about 6–7 samples per year) proved to be a sufficient sampling resolution to capture the full annual range of $\delta^{18}O$ variability in massive Porites corals (Quinn et al. 1996; Dassié and Linsley 2015).

Annual skeletal density bands for the corals analyzed in this study are not always distinct at every interval in a particular core; therefore, counting the number of growth bands (e.g., Knutson et al. 1972) is ineffective in making an accurate chronology. Clear annual cycles in

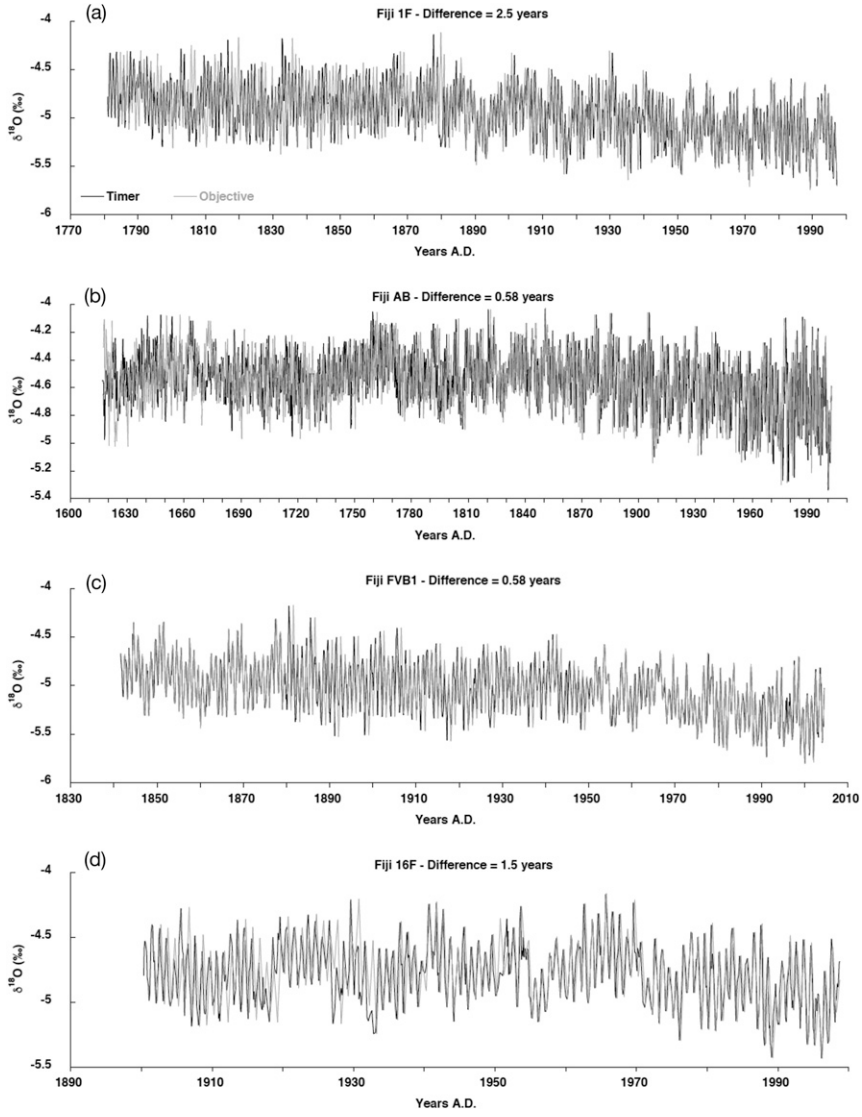

FIG. A1. (a)–(d) Fiji (1F, AB, FVB1, and 16F, respectively), (e)–(g) Tonga (TH1, TNI2, and TF1, respectively), and (h)–(j) Rarotonga (2R, 3R, and 99, respectively) time series chronologies made with the original (timer method in black) and objective (gray) methods. At the top of each panel, the values indicate the difference in years between the two age model determination methods (see appendix C and Table A1 for more details).

the millimeter-scale $\delta^{18}O$ FTR-region coral data allow for the construction of an accurate down-core chronology (see Ren et al. 2003; Linsley et al. 2004, 2006; Wu et al. 2013; Dassié et al. 2014). Lightest (most negative) $\delta^{18}O$ values in each seasonal cycle were attributed to the warmest month of the year, and the heaviest (most positive) values were attributed to the coldest. Prior to the instrumental SST record, the timing of seasonal SST minimum and maximum was assumed to be constant. Since the corals were alive when cored, the top age is assumed to represent the time of collection. Ages were assigned to specific depth increments and were then linearly interpolated into monthly intervals using a time series and spectral analysis application software package (ARAND; Howell et al. 2006). Chronologies were fine-tuned by cross-dating them at both seasonal and interannual time scales to the other records for the FTR region as well as to known ENSO events (see studies cited above for the initial description of each coral core). We developed an ''objective'' method based on automatic maxima and minima detection with some added conditions (appendix C) to quantify the chronology error. This method suggests that the age model error is less than 1 yr per 100 yr of core record (Fig. A1;

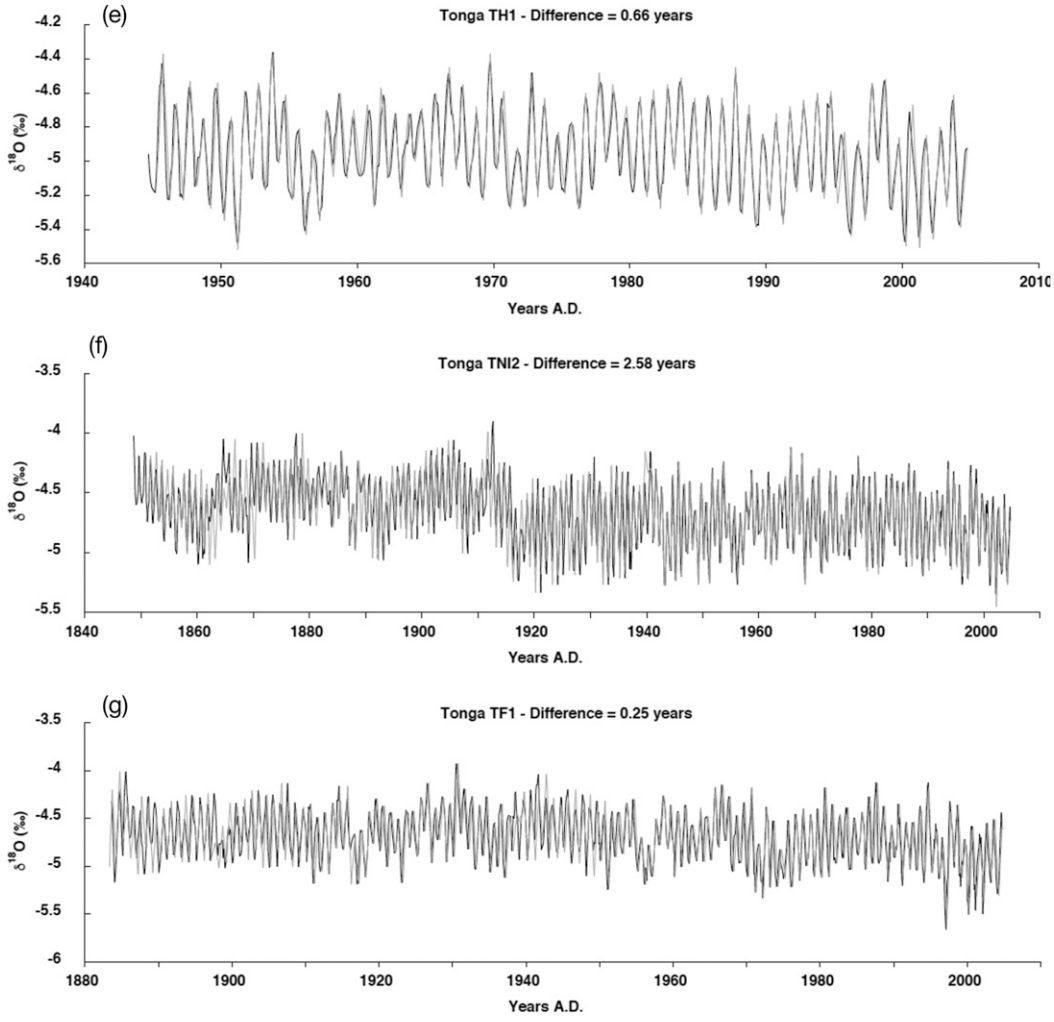

FIG. A1. (*Continued*)

Table A1). This error is lower than the error associated with the approach of counting density bands to develop an age model (e.g., DeLong et al. 2013), probably because of inconsistent density band formation and identification.

APPENDIX B

New Tonga Coral Record

The new coral core record, TF1, presented in this study was collected in 2004 on an exposed reef pass west of Fonoifua Island (20°16.750′S, 174°38.539′W). The colony was approximately 3 m high with approximately 7.5 m of water covering the top at low tide. TF1 was cut into about 7-mm-thick slabs along the maximum growth axis using a modified tile saw. The slabs were X-rayed (5 kV for 90 s) to determine the sampling tracks. Before sampling them, the slabs were cleaned in a deionized bath with a high-energy (500 W, 20 kHz) probe sonicator. The dried slabs were sampled using a low-speed micro drill with a 1-mm-round diamond drill bit along the maximum growth axis. A groove approximately 3 mm deep by approximately 3 mm wide was excavated at 1-mm increments. Approximately 100 μg of coral powder per sample was dissolved in about 100% H_3PO_4 at 90°C in a MultiPrep sample preparation device, and the generated CO_2 gas was analyzed by a Micromass Optima gas-source triple-collector mass spectrometer in the Stable Isotope Ratio Mass Spectrometer (SIRMS) Laboratory at the University at Albany, State University of New York. Over TF1 analytical time, the long-term precision of NBS-19 (laboratory standard) $\delta^{18}O$ was 0.05‰ (N = 123) and the average difference between replicates was 0.049‰ (N = 96).

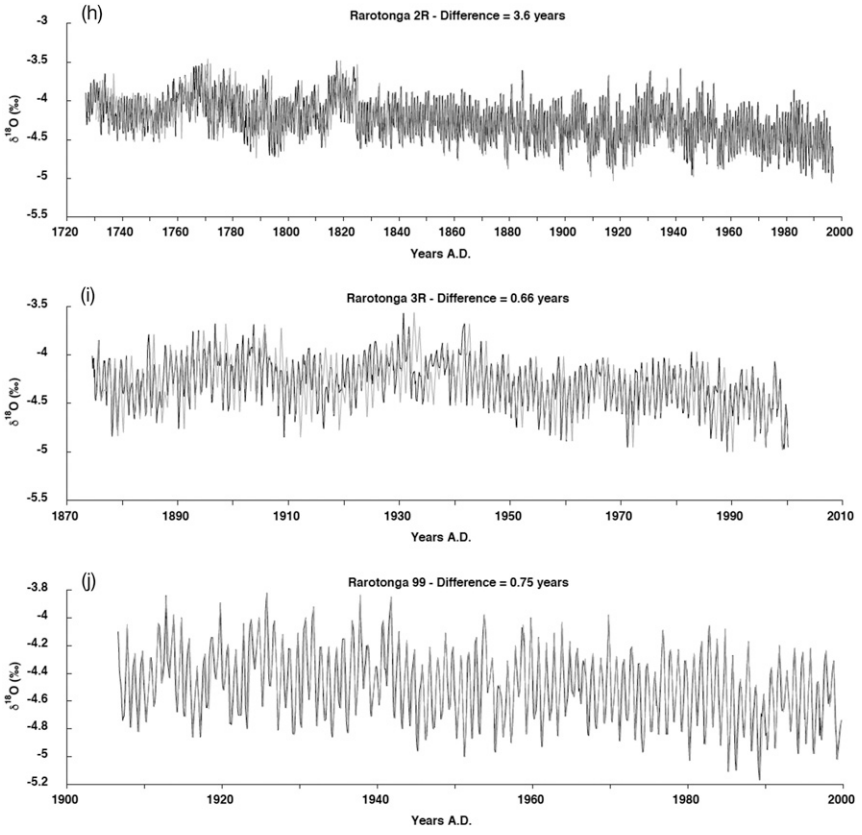

FIG. A1. (*Continued*)

APPENDIX C

Objective Coral Age Model Determination

We developed a method to determine in an objective and systematic manner the coral $\delta^{18}O$ time series age model. Results obtained by the "objective" method are then compared to the original age model determined by manually setting the timing of seasonal changes of geochemical proxy data (the "timer" method). The objective method is based on an R code that determines objectively the number of $\delta^{18}O$ seasonal cycles by first detecting the succession of maxima and minima in $\delta^{18}O$ time series corresponding to seasonal temperature minima and maxima, respectively. Based on the most recent known age of the $\delta^{18}O$ time series (coral being alive at time of collection), dates are then successively assigned to the detected coral $\delta^{18}O$ minima and maxima. To do so, we interpolate $\delta^{18}O$ values in order to obtain monthly time series, that is, six values between two consecutive minima and maxima. Time differences between the two methods are in months (see Table A1 and Fig. A1). The source code is available under GNU General Public License (https://github.com/lebasn/Corals).

APPENDIX D

Sea Surface Salinity Product Assessment

Two SSS products are presented in Fig. D1 and Table D1 and compared. The first SSS product, the observational Pacific Ocean gridded SSS product from Delcroix et al. (2011) (SSS_D), is a monthly resolution product covering the 1950–2008 period. It is an objective analysis

TABLE A1. The difference in years between the original and objective chronology methods.

Coral	Difference in yr	Total No. of yr	Difference for 100 yr
1F	2.5	216	1.16
AB	0.58	384	0.15
FVB1	0.58	163	0.36
16F	1.5	61	2.46
TF1	0.25	121	0.21
TH1	0.66	60	1.10
TNI2	2.58	156	1.65
2R	3.6	270	1.33
3R	0.66	126	0.52
99	0.75	93	0.81
Avg	—	—	0.97

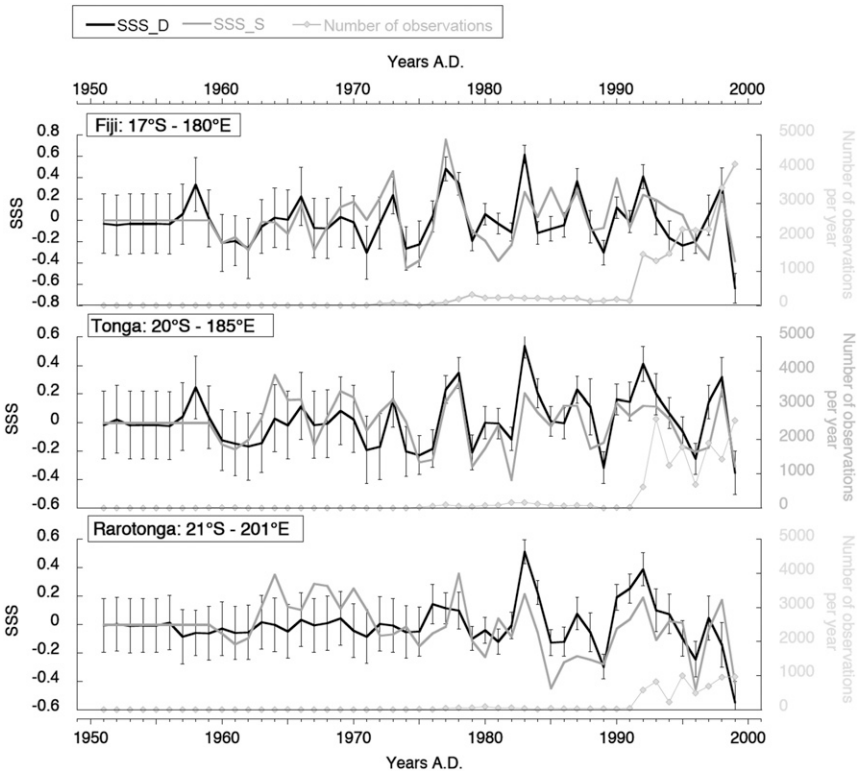

FIG. D1. Annual mean SSS time series (psu) for SSS_S (gray curve; Carton and Giese 2008) and SSS_D (black curve; Delcroix et al. 2011) products at (top)–(bottom) Fiji, Tonga, and Rarotonga. SSS_D associated error is shown as a gray curve with dots and corresponds to the number of observations per year. Both SSS_S and SSS_D time series were centered over the 1960–90 mean values.

of observations from Voluntary Observing Ships, Tropical Atmosphere Ocean/Triangle Trans–Ocean Buoy Network (TAO/TRITON) moorings, Argo float profiles, and conductivity–temperature–depth (CTD) casts. The density of observations in the SSS_D product is not spatially homogeneous (Fig. D2). For the neighboring grid points around Rarotonga, only 1000 observations were made between 1970 and 2000, whereas both Tonga and Fiji grids contain more than 20 000 observations. Error bars associated with the SSS_D product [defined by Delcroix et al. (2011) as the ''percentage of the variance of SSS anomalies relative to mean monthly climatology''] allow estimating the confidence we can place in the observed variability signal. This dataset uncertainty is linked to the number of observations per year (gray time series in Fig. D1). We decided to use data for which the associated error is below 0.2 psu (as recommended by Delcroix et al. 2011). Data prior to 1970, from the three sites, are therefore not considered for the remainder of this study.

The second SSS product, the SSS_S (Carton and Giese 2008;), is also a monthly product and covers the 1870–2010 period. It is based on data-assimilating numerical simulations. Data used for this product are obtained

TABLE D1. Annual mean SSS of SSS_D (Delcroix et al. 2011) and SSS_S (Carton and Giese 2008) mean values (psu), standard deviations, and errors calculated over the 1970–2000 period. The df used to evaluate the significance level for the correlation between SSS_D and SSS_S is shown in parentheses. All correlation coefficients are significant at the 99% confidence level.

	Fiji		Tonga		Rarotonga	
	SSS_D	SSS_S	SSS_D	SSS_S	SSS_D	SSS_S
Mean	35	34.74	35.27	34.87	35.52	35.04
Std dev	0.29	0.3	0.25	0.2	0.21	0.2
Estimated error mean	0.14	—	0.13	—	0.13	—
Correlation (df)	0.71 (35)	—	0.67 (35)	—	0.56 (39)	—

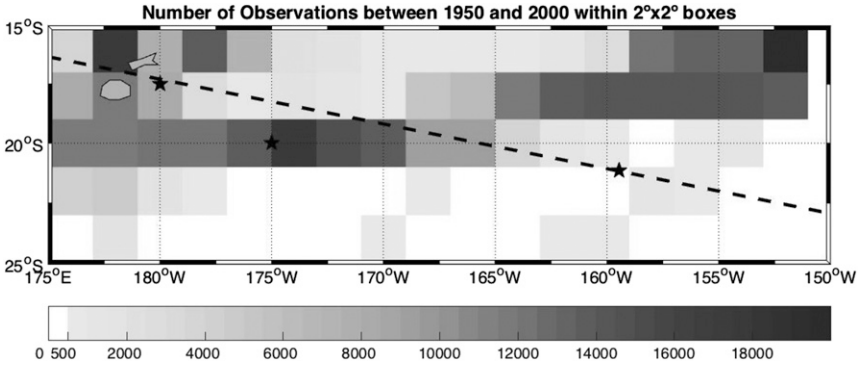

FIG. D2. Density map of the number of SSS ship observations over the 1950–2000 period used by Delcroix et al. (2011) to produce their SSS gridded product.

from the *World Ocean Atlas 2001* (Boyer et al. 2002). Systematic sampling of SSS (more than 10 000 observations per year globally) did not start until after 1960, and reached a steady state in the 1970s through the 1990s (Bingham et al. 2002). Despite not having associated errors, data prior to 1970 are therefore not considered in this study, owing to the sparse spatial and temporal observation sampling.

The two datasets, SSS_D and SSS_S, are not entirely independent, since they both use TAO/TRITON array, Argo data, and CTD cast data. The main difference arises from the methodology used to interpolate the data. SSS_D is based purely on observations, whereas SSS_S is based on model assimilation. We therefore believe comparison of the two products in the FTR region can be useful for evaluating SSS uncertainties for our region of study. For the areas associated with each coral site, annual-averaged SSS_D and SSS_S products show similar interannual variability timing over the 1970–2000 period (Fig. D1). They are significantly correlated at the 99% confidence level (Table D1) despite presenting different means (Student's *t* test with a 99% confidence level).

To help us determine which SSS product is better suited in our FTR region, we compared each coral composite δ^{18}O time series with the corresponding SSS_D and SSS_S time series at each site for the 1970–2000 overlapping period (Fig. D3). To be consistent with coral δ^{18}O composites, a 25-month Hanning filter (Blackman and Tukey 1958) is run on both instrumental SSS datasets. The correlation coefficient between coral δ^{18}O composites and SSS_D was 0.89 at Fiji and decreases to 0.75 at Tonga and 0.63 at Rarotonga (significant at the 99% confidence level). Most of the dissimilarities between coral δ^{18}O and SSS_D are, however, within the error limits of the gridded SSS (gray shading in Fig. D3). Correlation coefficients between δ^{18}O and SSS_S are 0.69 at Fiji, 0.49 at Tonga, and 0.58 at Rarotonga (significant at the 99% confidence level). Despite significant correlations between both SSS products (Table D1), correlations between coral δ^{18}O composites and SSS data are greater for SSS_D than SSS_S. This suggests that SSS_D is more suitable for this region and will be the only dataset used for the remainder of our study.

APPENDIX E

Evaluation of the Influence of Sea Surface Temperature and Salinity Colinear Variability on Coral δ^{18}O Time Series

a. Interannual time scale

Shallow water hermatypic coral δ^{18}O is known to be mainly a function of SSS and SST [see Corrège (2006) for review]. As discussed in the introduction, previous studies from the FTR region concluded that on interannual time scales, coral δ^{18}O is mainly affected by SSS variability (Le Bec et al. 2000; Linsley et al. 2006, 2008; Dassié et al. 2014). On interannual time scales, observed SST (ERSST.v4; Smith et al. 2008) and SSS (Delcroix et al. 2011) variability are significantly correlated at the 99% confidence level (−0.68, −0.59, and −0.48 for Fiji, Tonga, and Rarotonga, respectively). It is therefore not possible to separate the influence of SST and SSS on the coral δ^{18}O interannual variability. To determine the relative influence of SST and SSS variability on coral δ^{18}O composites, we compared monthly coral δ^{18}O time series (filtered with a 25-month Hanning filter) to "pseudocorals" time series. Pseudocorals correspond to modeled δ^{18}O time series based on the dependence of coral isotopic composition to SST ($-0.22‰\ °C^{-1}$) and SSS ($0.35‰\ psu^{-1}$) following the linear method described in Thompson et al. (2011). Two pseudocoral δ^{18}O time series, one based only on SSS and one based on both SST and SSS, were created.

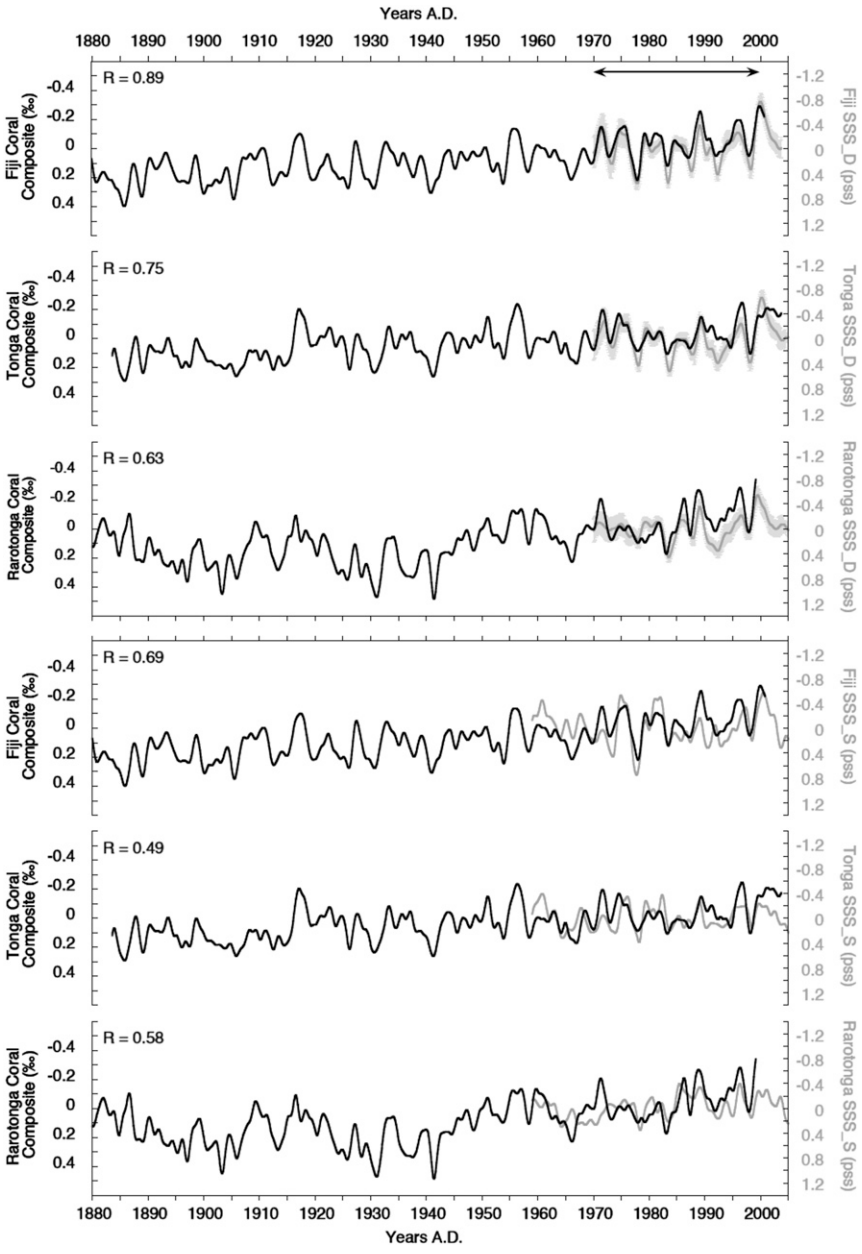

FIG. D3. Monthly time series after a 25-month Hanning filter of coral δ^{18}O composite values (black curve). (top) SSS_D (gray curve; Delcroix et al. 2011) and (bottom) SSS_S (gray curve; Carton and Giese 2008) for Fiji, Tonga, and Rarotonga, respectively (psu). The gray shading overlapping the gray curves in (top) corresponds to the error (maximal error estimation) associated with the SSS_D dataset. Correlation coefficient between coral δ^{18}O and observed SSS over the 1970–2000 period are given in the top-left corner of each panel. They are all significant at the 99% confidence level.

Correlation between coral δ^{18}O composites and modeled δ^{18}O based on SSS only or both SST and SSS are similar at all three sites and significant at the 99% confidence level. The addition of the SST factor into the modeled δ^{18}O time series does not increase the correlation between the modeled and coral δ^{18}O time series and therefore, does not add meaningful information. This suggests a dominant influence of SSS variability on coral δ^{18}O variability at interannual time scale.

b. *Secular scale*

At frequencies lower than interannual, the colinearity between SST and SSS cannot be assessed, since instrumental SSS only covers the last 30 years. We therefore

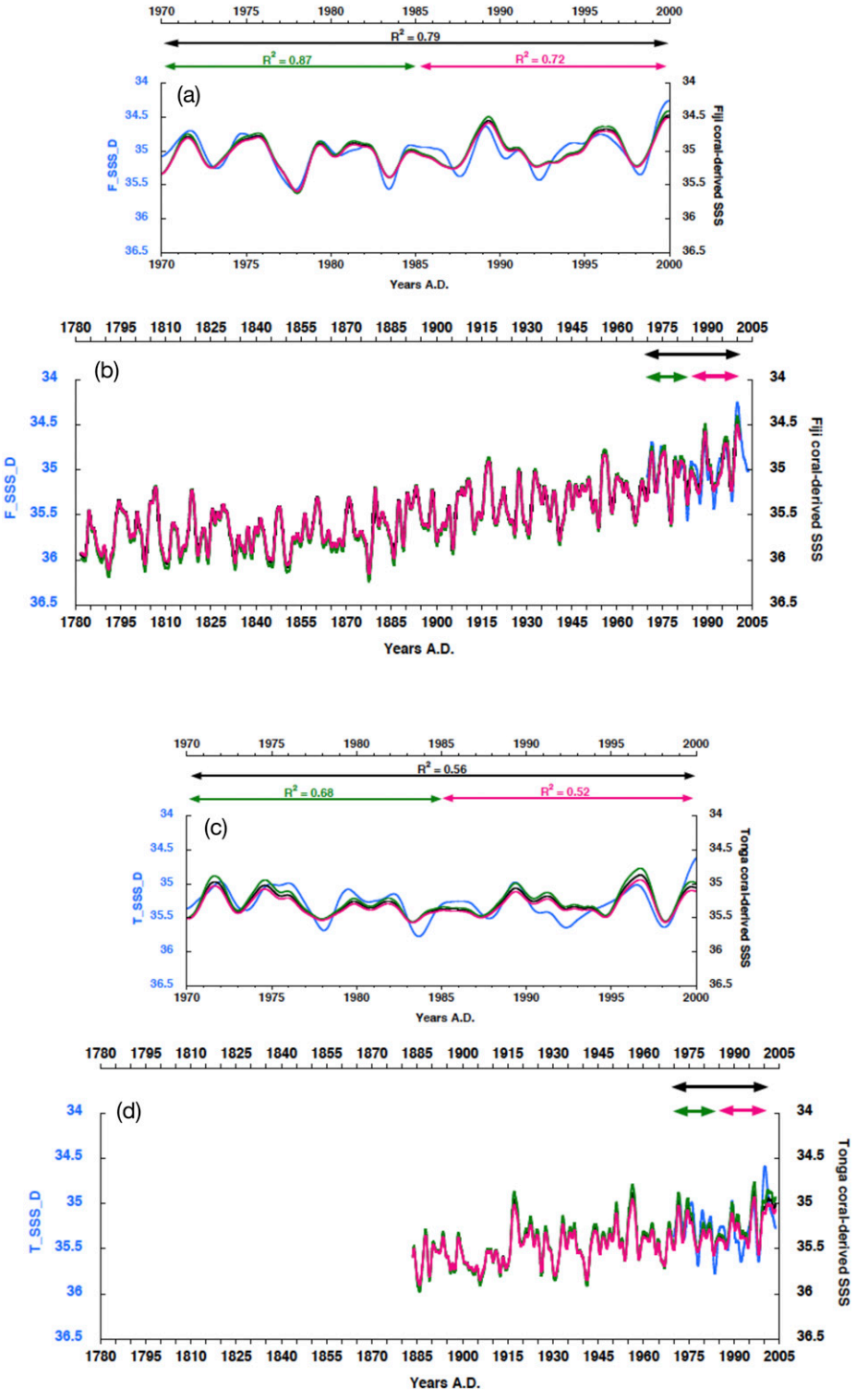

FIG. E1. Linear regression model predictions of SSS using (a),(b) Fiji, (c),(d) Tonga, and (e),(f) Rarotonga coral composites as predictors of the SSS_D dataset. Three periods are tested to calibrate the linear model: the 1970–2000 (black curve), 1970–85 (green curve), and 1985–2000 (pink curve) periods.

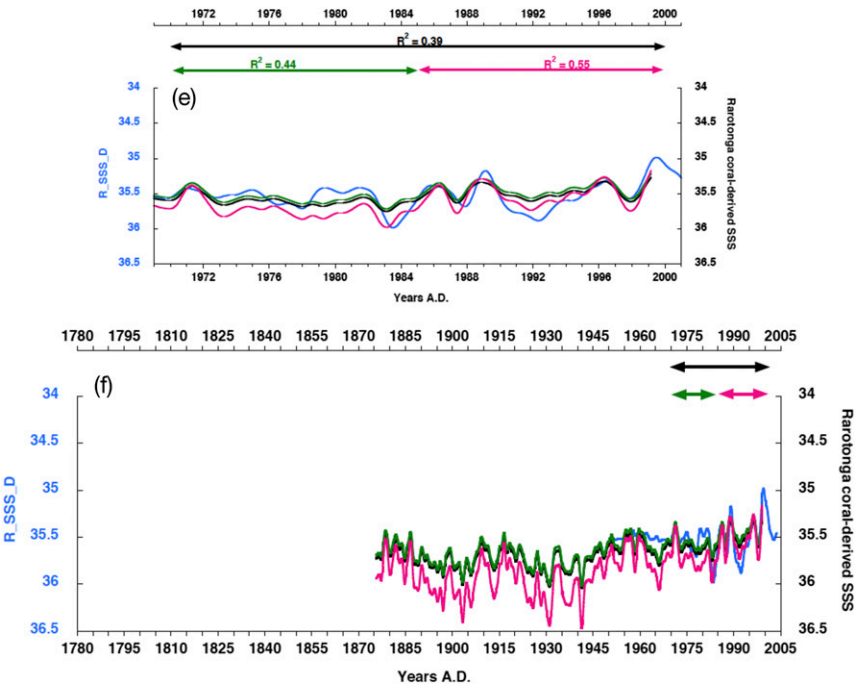

FIG. E1. (*Continued*)

constrain the long-term $\delta^{18}O$ trend by removing the influence of SST warming as if both SST and SSS trends were independent. Instrumental SST datasets (NOAA/NCDC ERSST.v4; see section 2b) indicate that the FTR region is influenced by a long-term warming trend that started around 1914 in all three sites. The warming corresponds to 0.028°, 0.017°, and 0.033°C decade^{-1} for Fiji, Tonga, and Rarotonga, respectively (Table 6). To attempt to constrain the amplitude of the twentieth-century freshening trend, we linearly remove the SST influence on the $\delta^{18}O$ long-term trend. Instrumental SSTs are converted into $\delta^{18}O_{SST}$ time series by exploiting the most commonly used $\delta^{18}O_{SST}$ slope of $-0.23‰$ °C^{-1} when comparing multiple locations (e.g., Epstein et al. 1953; Evans et al. 2000; Lough 2004; Thompson et al. 2011). The residual long-term $\delta^{18}O_{sw}$ trend ($\delta^{18}O - \delta^{18}O_{SST}$) is then converted into SSS variability ($\delta^{18}O_{sw}$-derived SSS) using the FTR-region linear models (Fig. E1 and Table E1). Over the 1970–2003 SSS observational period, Delcroix et al. (2007) found a linear SSS decreasing trend of −0.29 psu over the area 15°–17°S, 170°E–170°W. Over the 1970–99 period, using $\delta^{18}O$-derived SSS, we found a similar linear decreasing trend of −0.23 psu for Fiji, −0.22 psu for Tonga, and −0.17 psu for Rarotonga (Table 6). When using $\delta^{18}O_{sw}$-derived SSS time series at Fiji, the decreasing trend becomes −0.21 psu for

TABLE E1. Linear regression model fraction of explained variance R^2, slopes, and intercepts between FTR-region coral composite $\delta^{18}O$ and SSS_D over three different time periods: 1970–85, 1985–2000, and 1970–2000.

	Slope	Intercept	R^2
Fiji			
1970–85	0.365 652 ± 0.010 540	−0.036 992 ± 0.002 559	0.87
1985–2000	0.336 62 ± 0.015 766	−0.058 661 ± 0.003 921	0.72
1970–2000	0.356 676 ± 0.009 741	−0.047 385 ± 0.002 394	0.79
Tonga			
1970–85	0.303 037 ± 0.015 643	−0.029 238 ± 0.003 35	0.68
1985–2000	0.289 119 ± 0.021 021	−0.057 123 ± 0.004 639	0.52
1970–2000	0.290 876 ± 0.013 496	−0.043 106 ± 0.002 935	0.56
Rarotonga			
1970–85	0.244 688 7 ± 0.020 703 8	−0.000 231 7 ± 0.003 055 4	0.44
1985–2000	0.303 477 ± 0.020 834	−0.095 566 ± 0.003 917	0.55
1970–2000	0.315 150 ± 0.020 865	−0.047 905 ± 0.003 514	0.39

Fiji, −0.17 psu for Tonga, and −0.15 psu for Rarotonga (Table 6), values much weaker than those found using instrumental SSS. This leads us to conclude that both SST and SSS trends are not independent, and that we cannot remove the SST influence on the long-term $\delta^{18}O$ trend. The $\delta^{18}O$ and SSS relationship might change through time, but it should not be the case over the last 200 years. We therefore decide to focus only on $\delta^{18}O$-derived SSS in this study.

REFERENCES

Adler, R. F., and Coauthors, 2003: The Version-2 Global Precipitation Climatology Project (GPCP) monthly precipitation analysis (1979–present). *J. Hydrometeor.*, **4**, 1147–1167, https://doi.org/10.1175/1525-7541(2003)004<1147:TVGPCP>2.0.CO;2.

Bai, J., 1994: Least squares estimation of a shift in linear processes. *J. Time Ser. Anal.*, **15**, 453–472, https://doi.org/10.1111/j.1467-9892.1994.tb00204.x.

Bingham, F. M., S. D. Howden, and C. J. Koblinsky, 2002: Sea surface salinity measurements in the historical database. *J. Geophys. Res.*, **107**, 8019, https://doi.org/10.1029/2000JC000767.

Blackman, R. B., and J. W. Tukey, 1958: The measurement of power spectra from the point of view of communications engineering—Part I. *Bell Syst. Tech. J.*, **37**, 185–282, https://doi.org/10.1002/j.1538-7305.1958.tb03874.x.

Boyer, T. P., C. Stephens, J. I. Antonov, M. E. Conkright, R. A. Locarnini, T. D. O'Brien, and H. E. Garcia, 2002: *Salinity*. Vol. 2, *World Ocean Atlas 2001*, NOAA Atlas NESDIS 50, 165 pp.

Cai, W., and Coauthors, 2012: More extreme swings of the South Pacific convergence zone due to greenhouse warming. *Nature*, **488**, 365–369, https://doi.org/10.1038/nature11358.

Carton, J. A., and B. S. Giese, 2008: A reanalysis of ocean climate using Simple Ocean Data Assimilation (SODA). *Mon. Wea. Rev.*, **136**, 2999–3017, https://doi.org/10.1175/2007MWR1978.1.

Chou, C., J. D. Neelin, C.-A. Chen, and J.-Y. Tu, 2009: Evaluating the "rich-get-richer" mechanism in tropical precipitation change under global warming. *J. Climate*, **22**, 1982–2005, https://doi.org/10.1175/2008JCLI2471.1.

Corrège, T., 2006: Sea surface temperature and salinity reconstruction from coral geochemical tracers. *Palaeogeogr. Palaeoclimatol. Palaeoecol.*, **232**, 408–428, https://doi.org/10.1016/j.palaeo.2005.10.014.

Cravatte, S., T. Delcroix, D. Zhang, M. McPhaden, and J. Leloup, 2009: Observed freshening and warming of the western Pacific warm pool. *Climate Dyn.*, **33**, 565–589, https://doi.org/10.1007/s00382-009-0526-7.

Dassié, E. P., and B. K. Linsley, 2015: Refining the sampling approach for the massive coral *Diploastrea heliopora* for $\delta^{18}O$-based paleoclimate applications. *Palaeogeogr. Palaeoclimatol. Palaeoecol.*, **440**, 274–282, https://doi.org/10.1016/j.palaeo.2015.08.043.

——, ——, T. Corrège, H. C. Wu, G. M. Lemley, S. Howe, and G. Cabioch, 2014: A Fiji multi-coral $\delta^{18}O$ composite approach to obtaining a more accurate reconstruction of the last two-centuries of the ocean-climate variability in the South Pacific convergence zone region. *Paleoceanography*, **29**, 1196–1213, https://doi.org/10.1002/2013PA002591.

de Boyer Montégut, C., G. Madec, A. S. Fischer, A. Lazar, and D. Iudicone, 2004: Mixed layer depth over the global ocean: An examination of profile data and a profile-based climatology. *J. Geophys. Res.*, **109**, C12003, https://doi.org/10.1029/2004JC002378.

Delcroix, T., 1998: Observed surface oceanic and atmospheric variability in the tropical Pacific at seasonal and ENSO time scales: A tentative overview. *J. Geophys. Res.*, **103**, 18 611–18 633, https://doi.org/10.1029/98JC00814.

——, S. Cravatte, and M. J. McPhaden, 2007: Decadal variations and trends in tropical Pacific sea surface salinity since 1970. *J. Geophys. Res.*, **112**, C03012, https://doi.org/10.1029/2006JC003801.

——, G. Alory, S. Cravatte, T. Corrège, and M. J. McPhaden, 2011: A gridded sea surface salinity data set for the tropical Pacific with sample applications (1950–2008). *Deep-Sea Res. I*, **58**, 38–48, https://doi.org/10.1016/j.dsr.2010.11.002.

DeLong, K. L., T. M. Quinn, and F. W. Taylor, 2007: Reconstructing twentieth-century sea surface temperature variability in the southwest Pacific: A replication study using multiple coral Sr/Ca records from New Caledonia. *Paleoceanography*, **22**, PA4212, https://doi.org/10.1029/2007PA001444.

——, ——, ——, C.-C. Shen, and K. Lin, 2013: Improving coral-base paleoclimate reconstructions by replicating 350 years of coral Sr/Ca variations. *Palaeogeogr. Palaeoclimatol. Palaeoecol.*, **373**, 6–24, https://doi.org/10.1016/j.palaeo.2012.08.019.

Draper, N. R., and H. Smith, 1998: *Applied Regression Analysis*. 3rd ed. John Wiley and Sons, 736 pp.

Durack, P. J., S. E. Wijffels, and R. J. Matear, 2012: Ocean salinities reveal strong global water cycle intensification during 1950 to 2000. *Science*, **336**, 455–458, https://doi.org/10.1126/science.1212222.

Epstein, S., R. Buchsbaum, H. A. Lowenstam, and H. C. Urey, 1953: Revised carbonate-water isotopic temperature scale. *Geol. Soc. Amer. Bull.*, **64**, 1315–1326, https://doi.org/10.1130/0016-7606(1953)64[1315:RCITS]2.0.CO;2.

Evans, M. N., A. Kaplan, and M. A. Cane, 2000: Intercomparison of coral oxygen isotope data and historical sea surface temperature (SST): Potential for coral-based SST field reconstructions. *Paleoceanography*, **15**, 551–563, https://doi.org/10.1029/2000PA000498.

Folland, C. K., J. A. Renwick, M. J. Salinger, and A. B. Mullan, 2002: Relative influences of the interdecadal Pacific oscillation and ENSO on the South Pacific convergence zone. *Geophys. Res. Lett.*, **29**, 1643, https://doi.org/10.1029/2001GL014201.

Gagan, M. K., L. K. Ayliffe, D. Hopley, J. A. Cali, G. E. Mortimer, J. Chappell, M. T. McCulloch, and M. J. Head, 1998: Temperature and surface-ocean water balance of the mid-Holocene tropical western Pacific. *Science*, **279**, 1014–1018, https://doi.org/10.1126/science.279.5353.1014.

Ganachaud, A., and Coauthors, 2014: The southwest Pacific Ocean circulation and climate experiment (SPICE). *J. Geophys. Res. Oceans*, **119**, 7660–7686, https://doi.org/10.1002/2013JC009678.

Gouriou, Y., and T. Delcroix, 2002: Seasonal and ENSO variations of sea surface salinity and temperature in the South Pacific convergence zone during 1976–2000. *J. Geophys. Res.*, **107**, 8011, https://doi.org/10.1029/2001JC000830.

Guilderson, T. P., and D. P. Schrag, 1999: Reliability of coral isotope records from the western Pacific warm pool: A comparison using age-optimized records. *Paleoceanography*, **14**, 457–464, https://doi.org/10.1029/1999PA900024.

Hammer, Ø., D. A. T. Harper, and P. D. Ryan, 2001: Past: Paleontological statistics software package for education and data analysis. *Palaeontol. Electronica*, **4**, 1–9, http://palaeo-electronica.org/2001_1/past/past.pdf.

Hasson, A. E. A., T. Delcroix, and R. Dussin, 2013: An assessment of the mixed layer salinity budget in the tropical Pacific Ocean. Observations and modelling (1990–2009). *Ocean Dyn.*, **63**, 179–194, https://doi.org/10.1007/s10236-013-0596-2.

Held, I. M., and B. J. Soden, 2006: Robust responses of the hydrological cycle to global warming. *J. Climate*, **19**, 5686–5699, https://doi.org/10.1175/JCLI3990.1; Corrigendum, **24**, 1559–1560, https://doi.org/10.1175/2010JCLI4045.1.

Hill, K. L., S. R. Rintoul, K. R. Ridgway, and P. R. Oke, 2011: Decadal changes in the South Pacific western boundary current system revealed in observations and ocean state estimates. *J. Geophys. Res.*, **116**, C01009, https://doi.org/10.1029/2009JC005926.

Howell, P., N. Pisias, J. Ballance, J. Baughman, and L. Ochs, 2006: ARAND time-series analysis software. Brown University.

Kessler, W. S., and S. Cravatte, 2013: Mean circulation of the Coral Sea. *J. Geophys. Res. Oceans*, **118**, 6385–6410, https://doi.org/10.1002/2013JC009117.

Knutson, D. W., R. W. Buddemeier, and S. V. Smith, 1972: Coral chronometers: Seasonal growth bands in reef corals. *Science*, **177**, 270–272, https://doi.org/10.1126/science.177.4045.270.

Le Bec, N., A. Julliet-Leclerc, T. Corrège, D. Blamart, and T. Delcroix, 2000: A coral δ^{18}O record of ENSO driven sea surface salinity variability in Fiji (south-western tropical Pacific). *Geophys. Res. Lett.*, **27**, 3897–3900, https://doi.org/10.1029/2000GL011843.

Li, J., and Coauthors, 2013: El Niño modulations over the past seven centuries. *Nat. Climate Change*, **3**, 822–826, https://doi.org/10.1038/nclimate1936.

Linsley, B. K., G. M. Wellington, and D. P. Schrag, 2000: Decadal sea surface temperature variability in the subtropical South Pacific from 1726 to 1997 A.D. *Science*, **290**, 1145–1148, https://doi.org/10.1126/science.290.5494.1145.

——, ——, ——, L. Ren, M. J. Salinger, and A. W. Tudhope, 2004: Geochemical evidence from corals for changes in the amplitude and spatial pattern of South Pacific interdecadal climate variability over the last 300 years. *Climate Dyn.*, **22**, 1–11, https://doi.org/10.1007/s00382-003-0364-y.

——, A. Kaplan, Y. Gouriou, J. Salinger, P. B. deMenocal, G. M. Wellington, and S. S. Howe, 2006: Tracking the extent of the South Pacific convergence zone since the early 1600s. *Geochem. Geophys. Geosyst.*, **7**, Q05003, https://doi.org/10.1029/2005GC001115.

——, P. Zhang, A. Kaplan, S. S. Howe, and G. M. Wellington, 2008: Interdecadal-decadal climate variability from multicoral oxygen isotope records in the South Pacific convergence zone region since 1650 A.D. *Paleoceanography*, **23**, PA2219, https://doi.org/10.1029/2007PA001539.

——, H. C. Wu, E. P. Dassié, and D. P. Schrag, 2015: Decadal changes in South Pacific sea surface temperatures and the relationship to the Pacific decadal oscillation and upper ocean heat content. *Geophys. Res. Lett.*, **42**, 2358–2366, https://doi.org/10.1002/2015GL063045.

Liu, Y., X. S. Liang, and R. H. Weisberg, 2007: Rectification of the bias in the wavelet power spectrum. *J. Atmos. Oceanic Technol.*, **24**, 2093–2102, https://doi.org/10.1175/2007JTECHO511.1.

Lorrey, A., G. Dalu, J. Renwick, H. Diamond, and M. Gaetani, 2012: Reconstructing the South Pacific convergence zone position during the presatellite era: A La Niña case study. *Mon. Wea. Rev.*, **140**, 3653–3668, https://doi.org/10.1175/MWR-D-11-00228.1.

Lough, J. M., 2004: A strategy to improve the contribution of coral data to high-resolution paleoclimatology. *Palaeogeogr. Palaeoclimatol. Palaeoecol.*, **204**, 115–143, https://doi.org/10.1016/S0031-0182(03)00727-2.

Lumpkin, R., and G. C. Johnson, 2013: Global ocean surface velocities from drifters: Mean, variance, El Niño–Southern Oscillation response, and seasonal cycle. *J. Geophys. Res. Oceans*, **118**, 2992–3006, https://doi.org/10.1002/jgrc.20210.

Newman, M., and Coauthors, 2016: The Pacific decadal oscillation, revisited. *J. Climate*, **29**, 4399–4427, https://doi.org/10.1175/JCLI-D-15-0508.1.

O'Kane, T. J., D. P. Monselesan, and C. Maes, 2016: On the stability and spatiotemporal variance distribution of salinity in the upper ocean. *J. Geophys. Res. Oceans*, **121**, 4128–4148, https://doi.org/10.1002/2015JC011523.

Power, S., T. Casey, C. Folland, A. Colman, and V. Mehta, 1999: Inter-decadal modulation of the impact of ENSO on Australia. *Climate Dyn.*, **15**, 319–324, https://doi.org/10.1007/s003820050284.

Quinn, T. M., F. W. Taylor, T. J. Crowley, and S. M. Link, 1996: Evaluation of sampling resolution in coral stable isotope records: A case study using records from New Caledonia and Tarawa. *Paleoceanography*, **11**, 529–542, https://doi.org/10.1029/96PA01859.

Ren, L., B. K. Linsley, G. M. Wellington, D. P. Schrag, and O. Hoegh-Guldberg, 2003: Deconvolving the δ^{18}O seawater component from subseasonal coral δ^{18}O and Sr/Ca at Rarotonga in the southwestern subtropical Pacific for the period 1726 to 1997. *Geochim. Cosmochim. Acta*, **67**, 1609–1621, https://doi.org/10.1016/S0016-7037(02)00917-1.

Salinger, M. J., R. E. Basher, B. B. Fitzharris, J. E. Hay, P. D. Jones, J. P. Macveigh, and I. Schmidely-Leleu, 1995: Climate trends in the south-west Pacific. *Int. J. Climatol.*, **15**, 285–302, https://doi.org/10.1002/joc.3370150305.

——, J. A. Renwick, and A. B. Mullan, 2001: Interdecadal Pacific oscillation and South Pacific climate. *Int. J. Climatol.*, **21**, 1705–1721, https://doi.org/10.1002/joc.691.

——, S. McGree, F. Beucher, S. B. Power, and F. Delage, 2014: A new index for variations in the position of the South Pacific convergence zone 1910/11–2011/2012. *Climate Dyn.*, **43**, 881–892, https://doi.org/10.1007/s00382-013-2035-y.

Singh, A., T. Delcroix, and S. Cravatte, 2011: Contrasting the flavors of El Niño–Southern Oscillation using sea surface salinity observations. *J. Geophys. Res.*, **116**, C06016, https://doi.org/10.1029/2010JC006862.

Skliris, N., R. Marsh, S. A. Josey, S. A. Good, C. Liu, and R. P. Allan, 2014: Salinity changes in the World Ocean since 1950 in relation to changing surface freshwater fluxes. *Climate Dyn.*, **43**, 709–736, https://doi.org/10.1007/s00382-014-2131-7.

Smith, T. M., R. W. Reynolds, T. C. Peterson, and J. Lawrimore, 2008: Improvements to NOAA's historical merged land–ocean surface temperature analysis (1880–2006). *J. Climate*, **21**, 2283–2296, https://doi.org/10.1175/2007JCLI2100.1.

Stephans, C. L., T. M. Quinn, F. W. Taylor, and T. Corrège, 2004: Assessing the reproducibility of coral-based climate records. *Geophys. Res. Lett.*, **31**, L18210, https://doi.org/10.1029/2004GL020343.

Tchilibou, M., T. Delcroix, G. Alory, S. Arnault, and G. Reverdin, 2015: Variations of the tropical Atlantic and Pacific SSS minimum zones and their relations to the ITCZ and SPCZ rain bands (1979–2009). *J. Geophys. Res. Oceans*, **120**, 5090–5100, https://doi.org/10.1002/2015JC010836.

Terray, L., L. Corre, S. Cravatte, T. Delcroix, G. Reverdin, and A. Ribes, 2012: Near-surface salinity as nature's rain gauge to detect human influence on the tropical water cycle. *J. Climate*, **25**, 958–977, https://doi.org/10.1175/JCLI-D-10-05025.1.

Thompson, D. M., T. R. Ault, M. N. Evans, J. E. Cole, and J. Emile-Geay, 2011: Comparison of observed and simulated tropical climate trends using a forward model of coral $\delta^{18}O$. *Geophys. Res. Lett.*, **38**, L14706, https://doi.org/10.1029/2011GL048224.

Torrence, C., and G. P. Compo, 1998: A practical guide to wavelet analysis. *Bull. Amer. Meteor. Soc.*, **79**, 61–78, https://doi.org/10.1175/1520-0477(1998)079<0061:APGTWA>2.0.CO;2.

Tudhope, A. W., G. B. Shimmield, C. P. Chilcott, M. Jebb, A. E. Fallick, and A. N. Dalgleish, 1995: Recent changes in climate in the far western equatorial Pacific and their relationship to the Southern Oscillation; oxygen isotope records from massive corals, Papua New Guinea. *Earth Planet. Sci. Lett.*, **136**, 575–590, https://doi.org/10.1016/0012-821X(95)00156-7.

Vincent, D. G., 1994: The South Pacific convergence zone (SPCZ): A review. *Mon. Wea. Rev.*, **122**, 1949–1970, https://doi.org/10.1175/1520-0493(1994)122<1949:TSPCZA>2.0.CO;2.

Vincent, E. M., M. Lengaigne, C. E. Menkes, N. C. Jourdain, P. Marchesiello, and G. Madec, 2011: Interannual variability of the South Pacific convergence zone and implications for tropical cyclone genesis. *Climate Dyn.*, **36**, 1881–1896, https://doi.org/10.1007/s00382-009-0716-3.

Wu, H. C., B. K. Linsley, E. P. Dassié, B. Schiraldi, and P. B. deMenocal, 2013: Oceanographic variability in the South Pacific convergence zone region over the last 210 years from multi-site coral Sr/Ca records. *Geochem. Geophys. Geosyst.*, **14**, 1435–1453, https://doi.org/10.1029/2012GC004293.

Yu, L., 2007: Global variations in oceanic evaporation (1958–2005): The role of the changing wind speed. *J. Climate*, **20**, 5376–5390, https://doi.org/10.1175/2007JCLI1714.1.

——, 2011: A global relationship between the ocean water cycle and near-surface salinity. *J. Geophys. Res.*, **116**, C10025, https://doi.org/10.1029/2010JC006937.